International Journal of Physical Sciences

Volume 8 Number 25 9 July, 2013

ISSN 1992-1950

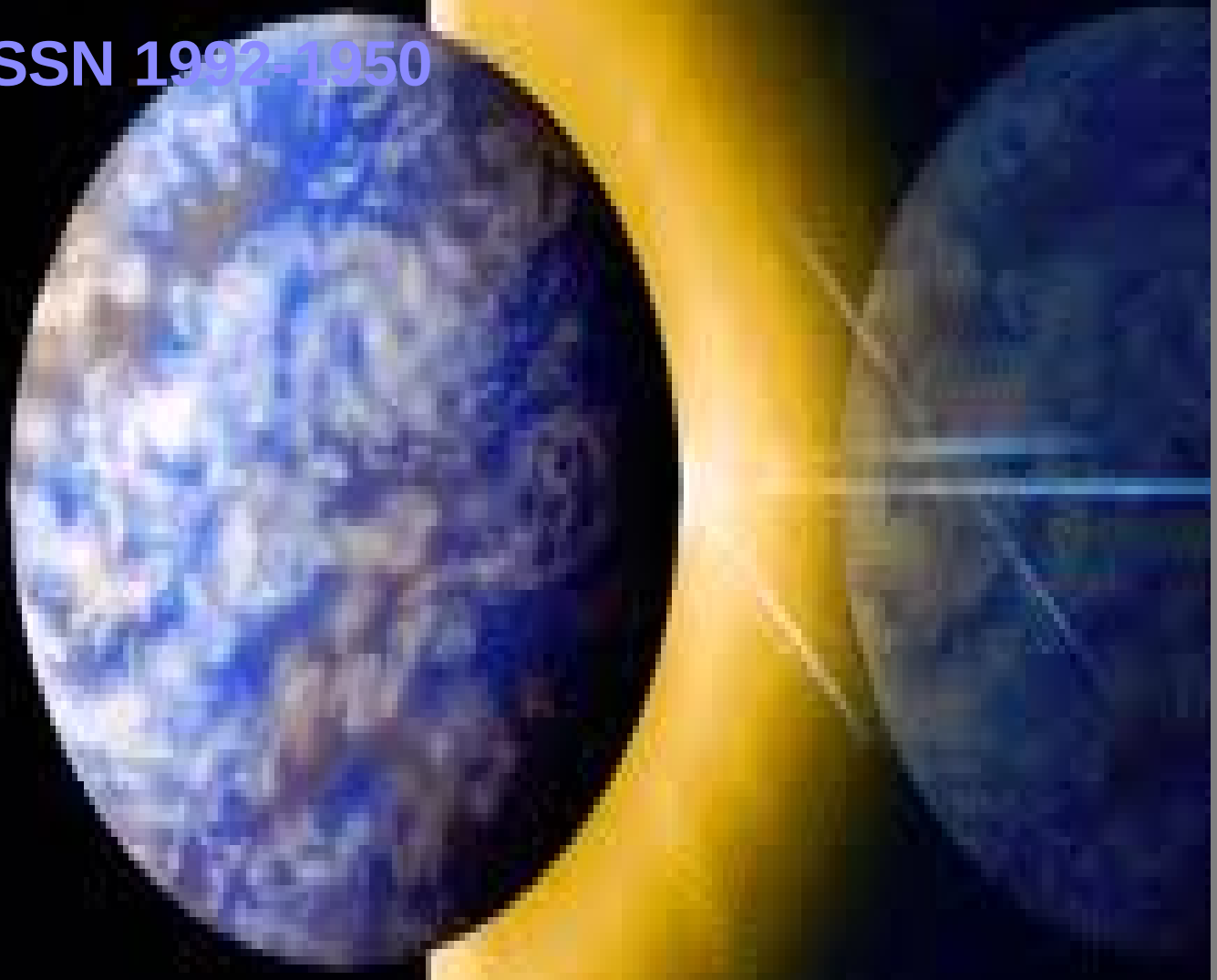

Academic Journals

ABOUT IJPS

The **International Journal of Physical Sciences (IJPS)** is published weekly (one volume per year) by Academic Journals.

International Journal of Physical Sciences (IJPS) is an open access journal that publishes high-quality solicited and unsolicited articles, in English, in all Physics and chemistry including artificial intelligence, neural processing, nuclear and particle physics, geophysics, physics in medicine and biology, plasma physics, semiconductor science and technology, wireless and optical communications, materials science, energy and fuels, environmental science and technology, combinatorial chemistry, natural products, molecular therapeutics, geochemistry, cement and concrete research, metallurgy, crystallography and computer-aided materials design. All articles published in IJPS are peer-reviewed.

Submission of Manuscript

Submit manuscripts as e-mail attachment to the Editorial Office at: ijps@academicjournals.org. A manuscript number will be mailed to the corresponding author shortly after submission.

For all other correspondence that cannot be sent by e-mail, please contact the editorial office (at ijps@academicjournals.org).

The International Journal of Physical Sciences will only accept manuscripts submitted as e-mail attachments.

Please read the **Instructions for Authors** before submitting your manuscript. The manuscript files should be given the last name of the first author.

Editors

Editorial Board

Instructions for Author

Electronic submission of manuscripts is strongly encouraged, provided that the text, tables, and figures are included in a single Microsoft Word file (preferably in Arial font).

The **cover letter** should include the corresponding author's full address and telephone/fax numbers and should be in an e-mail message sent to the Editor, with the file, whose name should begin with the first author's surname, as an attachment.

Article Types

Three types of manuscripts may be submitted:

Regular articles: These should describe new and carefully confirmed findings, and experimental procedures should be given in sufficient detail for others to verify the work. The length of a full paper should be the minimum required to describe and interpret the work clearly.

Short Communications: A Short Communication is suitable for recording the results of complete small investigations or giving details of new models or hypotheses, innovative methods, techniques or apparatus. The style of main sections need not conform to that of full-length papers. Short communications are 2 to 4 printed pages (about 6 to 12 manuscript pages) in length.

Reviews: Submissions of reviews and perspectives covering topics of current interest are welcome and encouraged. Reviews should be concise and no longer than 4-6 printed pages (about 12 to 18 manuscript pages). Reviews are also peer-reviewed.

Review Process

All manuscripts are reviewed by an editor and members of the Editorial Board or qualified outside reviewers. Authors cannot nominate reviewers. Only reviewers randomly selected from our database with specialization in the subject area will be contacted to evaluate the manuscripts. The process will be blind review.

Decisions will be made as rapidly as possible, and the journal strives to return reviewers' comments to authors as fast as possible. The editorial board will re-review manuscripts that are accepted pending revision. It is the goal of the IJPS to publish manuscripts within weeks after submission.

Regular articles

All portions of the manuscript must be typed double-spaced and all pages numbered starting from the title page.

The Title should be a brief phrase describing the contents of the paper. The Title Page should include the authors' full names and affiliations, the name of the corresponding author along with phone, fax and E-mail information. Present addresses of authors should appear as a footnote.

The Abstract should be informative and completely self-explanatory, briefly present the topic, state the scope of the experiments, indicate significant data, and point out major findings and conclusions. The Abstract should be 100 to 200 words in length.. Complete sentences, active verbs, and the third person should be used, and the abstract should be written in the past tense. Standard nomenclature should be used and abbreviations should be avoided. No literature should be cited.

Following the abstract, about 3 to 10 key words that will provide indexing references should be listed.

A list of non-standard **Abbreviations** should be added. In general, non-standard abbreviations should be used only when the full term is very long and used often. Each abbreviation should be spelled out and introduced in parentheses the first time it is used in the text. Only recommended SI units should be used. Authors should use the solidus presentation (mg/ml). Standard abbreviations (such as ATP and DNA) need not be defined.

The Introduction should provide a clear statement of the problem, the relevant literature on the subject, and the proposed approach or solution. It should be understandable to colleagues from a broad range of scientific disciplines.

Materials and methods should be complete enough to allow experiments to be reproduced. However, only truly new procedures should be described in detail; previously published procedures should be cited, and important modifications of published procedures should be mentioned briefly. Capitalize trade names and include the manufacturer's name and address. Subheadings should be used. Methods in general use need not be described in detail.

Results should be presented with clarity and precision. The results should be written in the past tense when describing findings in the authors' experiments. Previously published findings should be written in the present tense. Results should be explained, but largely without referring to the literature. Discussion, speculation and detailed interpretation of data should not be included in the Results but should be put into the Discussion section.

The Discussion should interpret the findings in view of the results obtained in this and in past studies on this topic. State the conclusions in a few sentences at the end of the paper. The Results and Discussion sections can include subheadings, and when appropriate, both sections can be combined.

The Acknowledgments of people, grants, funds, etc should be brief.

Tables should be kept to a minimum and be designed to be as simple as possible. Tables are to be typed double-spaced throughout, including headings and footnotes. Each table should be on a separate page, numbered consecutively in Arabic numerals and supplied with a heading and a legend. Tables should be self-explanatory without reference to the text. The details of the methods used in the experiments should preferably be described in the legend instead of in the text. The same data should not be presented in both table and graph form or repeated in the text.

Figure legends should be typed in numerical order on a separate sheet. Graphics should be prepared using applications capable of generating high resolution GIF, TIFF, JPEG or Powerpoint before pasting in the Microsoft Word manuscript file. Tables should be prepared in Microsoft Word. Use Arabic numerals to designate figures and upper case letters for their parts (Figure 1). Begin each legend with a title and include sufficient description so that the figure is understandable without reading the text of the manuscript. Information given in legends should not be repeated in the text.

References: In the text, a reference identified by means of an author‘s name should be followed by the date of the reference in parentheses. When there are more than two authors, only the first author‘s name should be mentioned, followed by ’et al‘. In the event that an author cited has had two or more works published during the same year, the reference, both in the text and in the reference list, should be identified by a lower case letter like ’a‘ and ’b‘ after the date to distinguish the works.

Examples:

Abayomi (2000), Agindotan et al. (2003), (Kelebeni, 1983), (Usman and Smith, 1992), (Chege, 1998; 1987a,b; Tijani, 1993,1995), (Kumasi et al., 2001)

References should be listed at the end of the paper in alphabetical order. Articles in preparation or articles submitted for publication, unpublished observations, personal communications, etc. should not be included in the reference list but should only be mentioned in the article text (e.g., A. Kingori, University of Nairobi, Kenya, personal communication). Journal names are abbreviated according to Chemical Abstracts. Authors are fully responsible for the accuracy of the references.

Examples:

Ogunseitan OA (1998). Protein method for investigating mercuric reductase gene expression in aquatic environments. Appl. Environ. Microbiol. 64:695-702.

Gueye M, Ndoye I, Dianda M, Danso SKA, Dreyfus B (1997). Active N2 fixation in several Faidherbia albida provenances. Ar. Soil Res. Rehabil. 11:63-70.

Charnley AK (1992). Mechanisms of fungal pathogenesis in insects with particular reference to locusts. In: Lomer CJ, Prior C (eds) Biological Controls of Locusts and Grasshoppers: Proceedings of an international workshop held at Cotonou, Benin. Oxford: CAB International, pp 181-190.

Mundree SG, Farrant JM (2000). Some physiological and molecular insights into the mechanisms of desiccation tolerance in the resurrection plant Xerophyta viscasa Baker. In Cherry et al. (eds) Plant tolerance to abiotic stresses in Agriculture: Role of Genetic Engineering, Kluwer Academic Publishers, Netherlands, pp 201-222.

Short Communications

Short Communications are limited to a maximum of two figures and one table. They should present a complete study that is more limited in scope than is found in full-length papers. The items of manuscript preparation listed above apply to Short Communications with the following differences: (1) Abstracts are limited to 100 words; (2) instead of a separate Materials and Methods section, experimental procedures may be incorporated into Figure Legends and Table footnotes; (3) Results and Discussion should be combined into a single section.

Proofs and Reprints: Electronic proofs will be sent (e-mail attachment) to the corresponding author as a PDF file. Page proofs are considered to be the final version of the manuscript. With the exception of typographical or minor clerical errors, no changes will be made in the manuscript at the proof stage.

International Journal of Physical Sciences

Table of Contents: Volume 8 Number 25 9 July, 2013

ARTICLES

academicJournals

Vol. 8(25), pp. 1334-1340, 9 July, 2013
DOI: 10.5897/IJPS2013.3802
ISSN 1992-1950 © 2013 Academic Journals
http://www.academicjournals.org/IJPS

International Journal of Physical Sciences

Full Length Research Paper

Assessment of arsenic levels in Guguletu and Langa rivers in Cape Town, South Africa

Akinsoji O.[1]*, Fatoki O. S.[1], Ximba B. J.[1], Opeolu B. O.[2] and Olatunji O. S.[1]

[1]Department of Chemistry, Cape Peninsula University of Technology, Bellville, South Africa.
[2]Department of Environmental and Occupational Studies, Cape Peninsula University of Technology, Cape Town, South Africa.

Accepted 8 July, 2013

This study investigates the baseline environmental levels of arsenic (As) in two rivers; one of which traverses through Guguletu (R_1) and the other running by the peripheral of Langa (R_2) residential areas in Cape Town. The rivers were monitored for As in upstream, midstream and downstream stations for twelve months, during consecutive summer and winter seasons between 2011 and 2012. The collected water samples were treated with HCl and KI, and heated in a water bath at 80°C for 30 min, and As was measured using hydride generation atomic absorption spectrometer (HG-AAS). The data obtained were subjected to descriptive statistics, while the Duncan Multiple Range tests was used to compare the mean concentrations of As in the different sampling stations, and between the two rivers. The mean concentration levels of arsenic ranged R_1, 0.98±0.34 to 1.23±0.43 (0.62 – 2.03) µg/L and 0.43±0.02 to 0.44±0.03 (0.08 – 0.68) µg/ℓ. The highest concentration of As (2.03 µg/ℓ) was observed in R_1 river water during summer, and the least concentration 0.08 µg/ℓ in R_2 water during winter. There was significant difference (P≤0.05) in the mean concentrations of As in R_1 and R_2 rivers water, while the seasonal mean concentrations during winter and summer, was not significantly different (P≥0.05). The concentrations of As detected in both rivers were lower than the recommended guideline value for freshwater.

Key words: Arsenic, concentration levels, seasonal, Guguletu and Langa rivers, Cape Town.

INTRODUCTION

Arsenic (As) occurs naturally in the environment; however the concentrations of arsenic can be elevated as a result of anthropogenic release, such as from mining and processing activities of variety of mineral ores such as copper, gold, nickel, lead, zinc etc, and during smelting metallurgical operations. Other anthropogenic sources of arsenic are from the use of arsenic containing insecticides and herbicides, combustion of wood treated with arsenic based preservative, seepages from hazardous waste sites, cotton and wool processing operations, and from coal combustion power generation plants, when arsenic contaminated coals are fired (Mondal et al., 2006).

Arsenic is mobilized and or remobilized by natural weathering reactions, biological activity, geochemical reactions, volcanic emissions and anthropogenic redistribution (Mohan and Pittman, 2007). Smedley et al. (2007); Smedley and Kinniburgh (2002) reported high arsenic levels in groundwater derived from zones of gold (Au) mineralization in the lower Proterozoic (Birimian) volcano-sedimentary rocks, where Au occurred along with quartz in its vein structures, and in altered sulphide minerals (pyrite, chalcopyrite, arsenopyrite). Soil erosion and leaching contribute between 6.12 × 1010

*Corresponding author. E-mail: snf_olatunji@ymail.com. Tel: +27822912934.

and 2.38 × 1011 g/year of arsenic in dissolved and suspended forms, respectively into the rivers and oceans (Mackenzie et al., 1979). Water bodies and drinking water sources may contain low concentration of anthropogenic or naturally occurring arsenic; however the level depends on the nature and source type. The increasing level of arsenic in water systems is of great concern all over the world due to human exposure via use of such water and its attendant effect on human and environment health.

The availability of arsenic in the environment arises from its persistence and ability to accumulate in different environmental compartment. The build-up of arsenic in the environment may result in toxic and deleterious consequences ranging from acute to chronic effects (IPCS, 2001; NRC, 2001; Some et al., 2012). The World Health Organization established that arsenic concentration greater than 10 µg/L in water, has adverse effect on human health (WHO, 2001). Studies revealed that skin disorder linked to the presence of arsenic in drinking water has been documented in many part of the world with the frequency of occurrence of the skin lesions associated with arsenic concentration in tube-well and groundwater (Charlet and Polya, 2006; Some et al., 2012). Elevated levels of arsenic in human blood causes skin disorders such as melanosis, keratosis and more rare skin tumour in contaminated populations (IPCS, 2001; Hashim et al., 2013). Other reported adverse effects of human exposure to arsenic include skin lesions, cardiovascular diseases, liver and kidney dysfunction cancer of the bladder, lungs, skin, kidney, nasal passages, liver, and prostate etc (NRC, 2001; Brinkel et al., 2009; Hashim et al., 2013).

The affinity of arsenic and selenium with gold, copper, nickel, zinc, lead, cobalt, silver and other ores mined in South Africa suggests that trace amount of arsenic may be widespread. Arsenic and selenium, unlike most other toxic metals and metalloids are fairly easily dissolved through a range of pH conditions and redox potential (Eh). This may lead to significant natural dissolution when high concentrations present in rocks and mineral formations are in contact with water. The use of As treated wood, or charcoal produced from the charring of As treated wood for domestic and commercial cooking, as well as other purposes such as braying, roasting, grilling and smoking in many homes and settlements in Cape Town and many part of South Africa, forms a major source of anthropogenic release and exposure of As. Information concerning the prevalence and distribution of arsenic in urban and rural rivers in Cape Town and its environs is scarce and scanty. There is need for the evaluation, characterization and prioritization of arsenic in the environment, in order to acquire basic data and critical information that may be required for developing policies, and making informed decision on environmental protection, management of arsenic contamination, as well as developing rational approach to mitigate the release of arsenic.

In this study, a systematic assessment on the sources, pathways and levels of arsenic in metropolitan streams and rivers traversing the Cape Town environment was investigated, in order to define the prevalence in Cape Town environment, and generate baseline data useful for monitoring purposes.

MATERIALS AND METHODS

Study area

Cape Town, the administrative seat of the Government of the Western Cape is located on the Western coast of South Africa geo-referenced on the Southern latitude S 33o and Eastern longitude E 18o. Outside the Cape Town city centre are a number of Peri-urban communities, settlements, and camps, many of which are populated beyond carriage capacity of the available residential. This meant the possibility of unsustainability use of available resources with high potential of negative consequences on the environment. The study covered stretch of major metropolitan rivers traversing through alternates of farmland and high density residential areas at Guguletu, (R_1) and offset areas of Langa (R_2) along Vanguard Road (Figure 1), which delivers urban sewerage into the central waste water treatment plant at Athlone, Cape Town environs.

The river flowing through Langa has its origin at the Southern area between Eppings Industrial Layout 1 and 2, traversing by the outskirt of the community. Industrial waste water released from the industries in Eppings 1 and 2 contributes significantly to the flow volume of the stream, and flow by the Athlone waste water treatment facility, releasing its content into Swart River which in-turn discharge it content in Atlantic Ocean in the North of the Peninsula. The river traversing Guguletu on the other hand, has it sourced from industrial waste water receiving pond at Belhar, traversing through the community, and with high human activities taking place around it. The Guguletu flow channels into Lotus River, which in-turn release it content into the Atlantic Ocean by the South of the Peninsula. Due to the high density residential through which both rivers flows, large quantity of domestic waste water, surface runoff and solid waste are added to the flowing waters.

At each of the rivers (Figure 1), water samples were collected at three different points marked as upstream, midstream and downstream. The geo-reference GPS co-ordinates for the Langa stream are; upstream (LS1) S 33° 56.698' E 18° 31.453', midstream (LS2) S 33° 56.994' E 18° 31.453 and downstream (LS3) S 33° 56.994' E 18° 30.500'. The GPS coordinates for Guguletu are upstream (GS1) S 33º 59.176´, E 18° 34.263´, midstream (GS2) S 33° 59.252´, E 18° 34.212´, downstream (GS3) S 33° 59.576´, and E 18º 34.055´.

Sample collection

Water samples were collected in pre-cleaned polyethylene containers. The containers were cleaned by soaking in a solution of 10% nitric acid and rinsed with deionized water. Samples were collected in triplicate from each sampling station along the rivers. Determination of physical and chemical properties of the water samples pH, conductivity, salinity and total dissolve solid (TDS).

The pH and conductivity of the water samples were determined in-situ using pre-calibrated Instrument (Hanna HI 4522), while water turbidity were measured with a pre-calibrated Turbidimeter 2100P. The salinity and total dissolve solid (TDS) of the water samples were determined according to methods prescribed by American Public Health Association (APHA, 1998). Recovery studies was

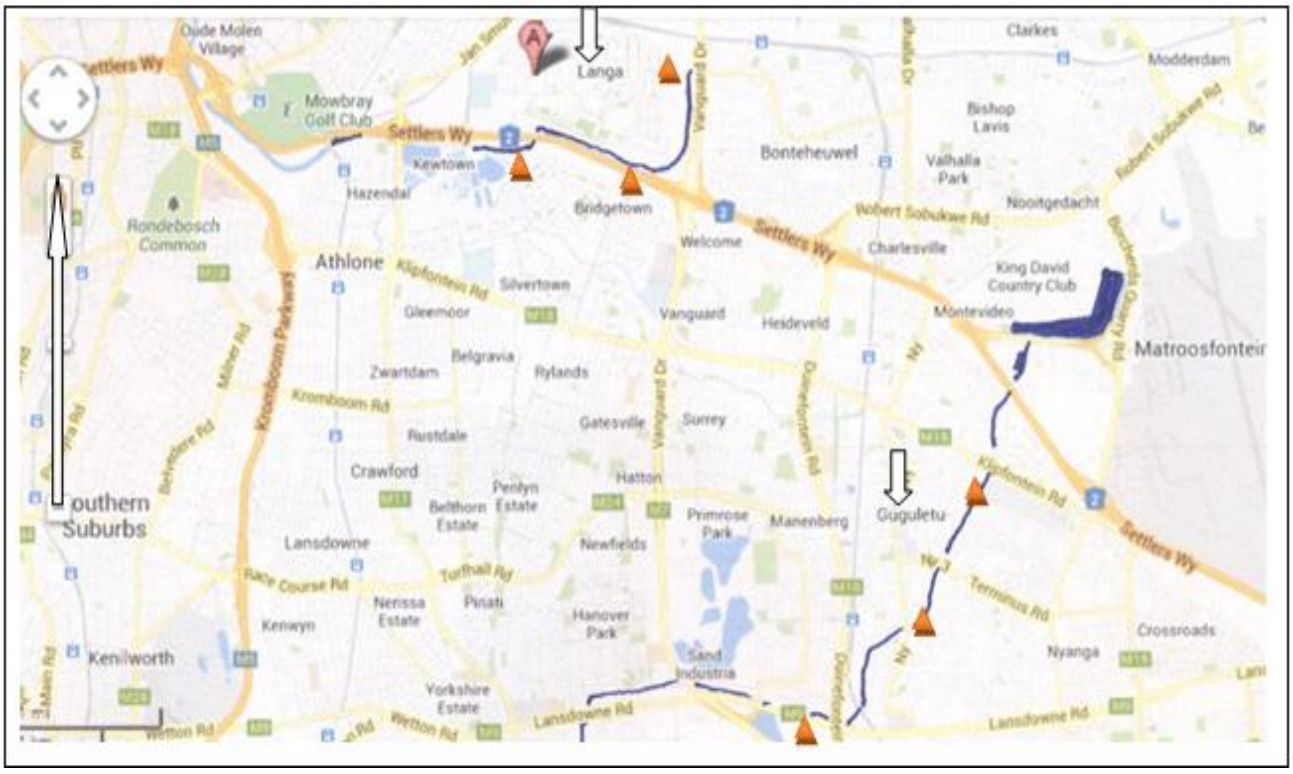

Figure 1. Map of Cape Town showing Guguletu and Langa study areas (Source: adapted from Google map). Legend: ▲ - Sampling Station; ⇩ - Study location.

also conducted on replicates (n=5) of spiked water samples and deionized water (n=5) to validate the efficiency of recovery of the method.

Sample preparation and estimation

Water samples were treated by the addition of 1 ml of 5 M HCl and 1 ml of 20% KI to a 10 mℓ water sample in test tubes and heated in a water bath at 80°C for 30 min (Wahed et al., 2006). The treated water were filtered into 50 ml volumetric flasks and made up to mark with deionized water. Procedural blank was prepared using the same method (Wahed et al., 2006), and aspirated to correct for background absorption. The concentrations of As were determined in the water samples using a Shimadzu atomic absorption spectrophotometer (AA–6300), coupled with a Hydride Vapour generator HVG-1 (HG- AAS) in stream of argon gas, at 0.32±0.02 MPA and a flow rate of 70 ml/min.

Recovery studies

Water samples and deionized water were spiked with different concentrations of As in 5- replicates. The spiked water samples and deionized water were subjected to sample preparation procedures, followed by the estimation of As in each of them.

RESULTS

The analysis of replicates spiked water samples and deionized water (n=5) showed good recovery between 100.3 to 104.4% and relative standard deviation of 3.21 to 12.42%. The percentage recoveries and relative standard deviation for arsenic (As) were 100.3 and 3.21% for spiked water; 104.4 and 12.42% for deionized water. The percentage recovery of As falls within the generally acceptable recovery 100±20%.

The mean concentration level of As in the water samples collected upstream (GS1, LS1), midstream (GS2, LS2) and downstream (GS3, LS3) at Guguletu (R_1) and Langa (R_2) were ranged 0.98±0.34 – 1.23±0.43 (0.62 – 2.03) µg/ℓ and 0.43±0.0.15 - 0.44±0.03 (0.08 – 0.68) µg/ℓ, respectively (Table 1). The highest concentration of As, 2.03 µg/L was observed in water collected from R_1 during summer, while the least concentration 0.08 µg/ℓ was measured in water collected from R_2 during winter.

The pH of R_1 water ranged between 6.7 upstream during winter and 8.4 midstream, during summer, while it ranged between 6.0 midstream during winter and 8.8 midstream during summer in R_2 river water. However, the mean pH of water measured at the different sampling stations along the rivers at R_1 and R_2 were 7.53±0.43 to 7.77±0.66 and 7.47±0.42 to 8.07±0.53, respectively (Table 1). The highest conductivity 1.67 mS/cm was measured in upstream water at R_1 during winter, with the least conductivity 0.49 mS/cm in downstream water at R_2 during winter as well. The mean conductivity of

Table 1. Result of selected physico-chemical properties and mean concentration (ug/l) of arsenic in water samples from the different sampling station along river course.

Sampling station	pH	Conductivity (mS/cm)	Turbidity (NTU)	Total dissolve solid (mg/L)	As (µg/L)
Guguletu					
Upstream	7.58±0.60	1.23±0.33	23.74±28.93	595.35±169.02	1.15±0.39
Midstream	7.58±0.12	1.06±0.50	44.33±33.99	530.27±248.86	0.87±0.18
Downstream	7.63±0.06	0.71±0.16	14.00±0.00	306.37±17.77	0.69±0.05
Overall mean	7.59±0.49	1.13±0.40	27.23±29.42	548.78±197.42	1.04±0.36
Summer	7.77±0.66	1.37±0.17	5.93±5.57	682.83±88.37	1.23±0.43
Winter	7.53±0.43	1.06±0.42	33.32±30.70	510.48±204.41	0.98±0.34
Mean	7.59±0.49	1.13±0.39	27.23±29.42	548.78±197.42	1.04±0.37
Langa					
Upstream	7.78±0.04	0.82±0.34	19.75±0.42	409.07±169.98	0.54±0.08
Midstream	7.59±0.62	0.95±0.26	17.29±14.30	471.98±132.45	0.47±0.10
Downstream	7.38±0.12	0.75±0.18	13.99±5.97	376.87±92.41	0.25±0.13
Overall mean	7.59±0.50	0.88±0.27	17.12±11.38	440.37±135.63	0.43±0.14
Summer	8.07±0.53	0.97±0.07	6.29±3.78	482.87±35.60	0.44±0.03
Winter	7.47±0.42	0.86±0.30	19.83±11.04	429.75±149.43	0.43±0.15
Mean	7.59±0.50	0.88±0.27	17.12±11.37	440.37±135.63	0.43±0.14

the water collected from the rivers at the different sampling stations ranged 1.06±0.42 mS/cm during winter to 1.37±0.17 mS/cm (Table 1) during summer at R_1, while that at R_2 ranged from 0.86±0.30 mS/cm to 0.97±0.07 mS/cm during winter and summer seasons, respectively.

The mean turbidity of the water samples were 5.93±5.57 - 33.32±30.70 NTU and 6.29±3.78 - 19.83±11.04 NTU in R_1 and R_2, during summer and winter seasons, respectively (Table 1). The lowest and highest water turbidity value of 0.37 NTU and 89.2 NTU were detected upstream at R_1 during summer and winter, respectively. The mean total dissolved solids (TDS) in water samples collected at the different sampling stations at R_1 and R_2 ranged 510.48±204.41 to 682.83±88.37 ppm and 429.75±149.43 to 482.87±35.60 ppm, respectively (Table 1). The lowest and highest TDS, 277.4 and 836.6 ppm were measured midstream at R_2 and upstream at R_1, respectively during winter. Generally, TDS detected in R_2 stream water ranged 277.4 - 779.5 ppm midstream, while TDS ranged 288.7 - 836.9 ppm in R_1 river.

DISCUSSION

The concentration of As varied between sampling stations in the upstream, midstream and downstream water courses; 0.62 - 2.03 µg/ℓ in the river traversing Guguletu (R_1) and 0.08 - 0.68 µg/ℓ in river running the peripherals of Langa (R_2). The variation in concentration levels of As depends on the physico-chemical properties of water, exposure of the rivers to either natural or anthropogenic source inputs and the chemical form of As in the rivers. In water, the concentration of As depends on the prevalence of AsIII oxide (As_2O_3), however the predominating form of As is a function of the water pH and redox conditions. For instance AsV oxide (HAs_2O_2-) is prevalent in water at circum - neutral pHs. In oxidizing or acidic water environment, As_2O_3

tends to form hydrated oxide (or arsenious acid), thereby decreasing the free and measurable As (As_2O_3) concentration. The concentration of As will therefore increase until at high pH, or strongly reducing water environment when ortho-arsenite (AsO33-) and meta-arsenite AsO_2- (that is, arsenites which are readily oxidized to arsenates) are formed from the reduction of As_2O_3 (Welch et al., 2000; Smedley and Kinniburgh, 2002; Charlet and Polya, 2006). There were significant differences ($P \leq 0.05$) in the levels of As detected in water samples collected at the different sampling stations in R_1 and R_2. This may be as a result of differences in volume and quantity of municipal and industrial runoff discharged into the main stream course, from adjoining settlements and industrial layouts at different intersections. According to EPA (1998), municipal waste water systems and septic tank in unsewered areas can contributes significant quantities of metals especially arsenic, mercury, chromium, lead, iron, manganese and biodegradable organic carbon to streams and rivers into which they empty their content. Exposure of surface water (especially those with sources from rocks/springs) or groundwater to geological sources rocks containing As minerals, and the nature of the hydrogeology of the water along the stream flow course as well as environmental factors can also exacerbate As levels. There may also be geological or anthropogenic hot spots, where higher levels of arsenic may occur along the river course (UNICEF, 2008). Human population and the food chain can inadvertently be exposed by drinking or using As-contaminated water (NRDC, 2000).

The concentrations of As detected in R_1 and R_2 waters were however below the 10 µg/L (0.010 ppm) maximum contaminant guideline level (MCL) set by World Health Organization (2001), however chronic exposure to lower levels of As is linked to adverse health effects in human populations. For instance, waters from tubes wells in some countries such as Bangladesh, Cambodia, Vietnam, Argentina, Chile, USA, Canada, Japan etc were reported to contain As at concentration levels that poses unacceptable risks (Hutton, 1987; Hashim et al., 2013). Although, As levels in the river systems were not detected at concentrations above the MCL, a maximum contaminant level goal (MCLG) of 0 ppm in water is recommended in order to avoid these adverse consequences (EPA, 1989). The concentration of As in R_1 water were higher compared to R_2 water, and this may be attributed to the proximal of R_1 river flow course to the Braai Centre at Guguletu, from where ash produced from open commercial meat roasting are washed into the main stream drainage, as well as other human activities such as the direct loading of combustion ash and other wastes into river.

The availability and prevalence of metals and many toxic substances in water systems, depends on the exposure of the water body to metals/toxic substances sources, the level they are exposed to, and the physico-chemical properties (pH, dissolved solids (TDS), turbidity conditions) of the water. The concentration of As varied with the pH of the river water at the different sampling stations (6.7 - 8.4 and 6.0 - 8.8 at R_1 and R_2, respectively), with higher As concentration observed as pH increased. Welch et al. (2000) reported that the concentration of As_2O_3 increases with increase in pH, and appeared to be constant at near neutral pH. The pH detected in the different sampling stations along the course of each of the rivers traversing Guguletu and Langa were not significantly different ($P \geq 0.05$). The observed conductivities of the waters in the different sampling stations in R_1 and R_2 at Guguletu and Langa were also not significantly different ($P \geq 0.05$). The ANZECC (2000) guideline (recommends that water pH should be within the range of 6.5 - 8.0 in healthy freshwater fit for sustenance of aquatic life and human health, while the South African Department of Water Affairs and Forestry and WHO water guideline standards (DWF, 1996) suggests a pH of range 6.0 – 9.0 for water used for domestic purposes.

Although, no definite relationship was established between pH and TDS (510.48±204.41 to 682.83±88.37 mg/l and 429.75±149.43 to 482.87±35.60 mg/l, in R_1 and R_2, respectively), results showed that the concentration of TDS increases with decrease in water pH. The conductivity of stream water (1.06±0.42 to 1.37±0.17 mS/cm and 0.86±0.30 to 0.97±0.07 mS/cm in R_1 and R_2, respectively) also increases with increase in TDS. The concentration of As also increases with increase in conductivity of the river water (with correlation coefficient γ=0.73 and γ=0.49 at R_1 and R_2, respectively). The conductivity of the water collected from all the sampling stations in R_1 and R_2 at Guguletu and Langa were higher than the 0.5 mS/cm, WHO recommended guideline limit for conductivity in water (Agbalagba et al., 2011).

Aside from insoluble substrates and particulates which may remain suspended in water, the turbidity of water is a function of the dynamics of water saturation and its capacity for dissolved solids. Guguletu river water showed higher turbidity (5.93±5.57 to 33.32±30.70 NTU) than R_2 at Langa (6.29±3.78 to 19.83±11.04 NTU). There is evidence of good correlation between water turbidity and TDS with correlation coefficient γ=0.68 and γ=0.54 for Guguletu and Langa river waters, respectively. This implies that turbid waters have high propensity for soluble metals than highly turbid water. On the other hand, it was reported that highly turbid waters tend to undergo self-purification by depositing excess particulate load in siltation and sedimentation process or as tidal deposits in flowing waters.

The turbidity of the water upstream, midstream and downstream were not significantly different ($P \geq 0.05$), although midstream turbidity was slightly higher probably because of human activities taking place about midstream. This study result is consistent with the findings of Amraoui et al. (2003) on turbidity dynamics in

Karstic systems of Ribaa and Bittit springs in the Middle Atlas (Morocco), Rowe et al. (2003), and Engstrom-Ost and Candolin (2006). Apart from a few samples (7.35%) where the turbidity of the water were less than 5 NTU during summer, all samples had turbidity values higher than the acceptable level, an indication of poor freshwater quality. The turbidity of the water in the two rivers were however not significantly different (P≥0.05).

The concentrations of arsenic were noted to be higher during summer than in winter. The low concentration of arsenic observed during winter may due to dilution, although this (dilution) may not totally account for the seasonal variation due to the likelihood of other arsenic reactions. The physico-chemical properties of the streams also varied with season. The pH, conductivity and TDS of the streams were higher during summer (dry season) than in during winter (wet season) while water turbidity was lower during summer (dry season). This is consistent with the findings of Ezekiel et al. (2011) on seasonal effect of pH condition of water measured in Sombreiro River. The conductivity, TDS, and salinity measured in water samples collected from Guguletu were also significantly (P≤0.05) higher than in water collected from Langa during both seasons.

The changing physico-chemical properties, such as TDS, conductivity, pH and redox potential, as well as flow volume and seasonal variations may probably explain the slight variation in the detected level As between different sampling stations on the rivers. The form and characteristics of occurrence in the water also have an effect on the available concentration levels. Thus, constant and consistent monitoring of water systems is desirable.

Conclusion

The concentration of As in the river waters were not appreciably high and within background levels. There were slight concentration levels variations in spatial distribution of arsenic in both river waters. Arsenic concentration levels in water samples were lower than the guideline minimum standard limit set by WHO, hence are below compliance level. The observed levels may serve as baseline data needed for environmental prioritization of arsenic prevalence in surface waters, since the observed concentration levels are not at a critical health thresholds limit. There is also need to develop national benchmark level for environmental monitoring against the buildup of As in streams and rivers in order to forestall exposure and adverse health effects in human populations.

REFERENCES

Agbalagba OE, Agbalagba OH, Ononugbo CP, Alao AA (2011). Investigation into the physico-chemical properties and hydrochemical processes of groundwater from commercial boreholes In Yenagoa, Bayelsa State, Nigeria. Afr. J. Environ. Sci. Technol. 5(7):473-481.

Amraoui F, Razack M, Bouchaou L (2003). Turbidity dynamics in Karstic systems: Example of Ribaa and Bittit springs in the Middle Atlas (Morocco). Hydrolog. Sci. J. 48(6):971-984.

ANZECC (2000). National Water Quality Management strategy:An introduction to the Australian and New Zealand guidelines for fresh and marine water quality. National water quality management strategy; No. 4a.

APHA (1998). Standard methods for the Examination of Water and Wastewater. 1268p 20th Ed. American Public Health, Association (APHA), American Water Works Association (AWWA), Water Pollution Control Federation (WPCF), Washington DC, USA.

Brinkel J, Khan MMH, Kraemer A (2009). A systematic review of arsenic exposure and its social and mental health effects with special reference to Bangladesh. Int. J. Environ. Res. Publ. Health 6:1609-1619.

Charlet L, Polya DA (2006). Arsenic in shallow, reducing ground waters in Southern Asia:an environmental health disaster. Elements 2:91-96.

DWF (Department of Water Affairs and Forestry) (1996). South African Water Quality Guidelines (second edition). Volume 1: Domestic Use.

Engstrom-Ost J, Candolin U (2006). Human-induced water turbidity alters selection on sexual displays in sticklebacks. Behavioral Ecology. Adv. Access Publ. pp. 393-398.

EPA (1989). Risk assessment guidance for superfund, Vol. 1: Human health evaluation manual Part A., interim final. Office of Emergency and Remedial Response, US Environmental Protection Agency, Washinghton DC, EPA/540/1-89/002.

EPA (1998). U.S. Environmental Protection Agency:Health Effects Test Guidelines, OPPTS 870.3250, 90-Day Dermal Toxicity.

Ezekiel EN, Hart AI, Abowei JFN (2011). The physical and chemical condition of Sombreiro River, Niger Delta, Nigeria. Res. J. Environ. Earth Sci. 3(4):327-340.

Hashim JH, Radzi RSM, Aljunid SM, Nur AM, Ismail A, Baguma D, Sthiannopkao S, Phan K, Wong MH, Sao V, Yasin MSM (2013). Hair arsenic levels and prevalence of arsenicosis in three Cambodian provinces. Sci. Tot. Environ. Article in press.

Hutton M (1987). Human health concerns of lead, mercury, cadmium and arsenic: In lead mercury, cadmium and arsenic in the environment, edited by TC Hutchinson and K Meema, Scope published by John Wiley and Sons Ltd.

IPCS (International Programme on Chemical Safety) (2001). Environmental Health Criteria 224: Arsenic and arsenic compounds. Geneva: World Health Organization.

Mackenzie ET, Lamtzy RJ, Petorson V (1979). Global trace metals cycles and predictions. J. Int. Assoc. Math. Geol. 6:99-142.

Mohan D, Pittman CU Jr. (2007). Arsenic removal from water/wastewater using adsorbents - A critical review. J. Hazard. Mat. 142:1-53.

Mondal P, Majumder CB, Mohanty B (2006). Laboratory based approaches for arsenic remediation from contaminated water:recent developments. J. Hazard. Mat. B. 137:464-479.

NRC (National Research Council) (2001). Arsenic in drinking water 2001 update. Washington DC; National Academy Press.

Rowe M, Essig D, Jessup B (2003). Guide to selection of sediment targets for use in Idaho TMDLs USEPA.

Smedley PL, Kinniburgh DG (2002). A Review of the source, behaviour and distribution of arsenic in natural waters. Appl. Geochem. 17:517-568.

Smedley PL, Knudsen J, Maiga D (2007). Arsenic in groundwater from mineralized proterozoic basement rocks of Burkina Faso. Appl. Geochem. 22:1074-1092.

Some IT, Sakira AK, Ouedraogo M, Ouedraogo TZ, Traore A, Sondo B, Guissou PI (2012). Arsenic levels in tube-wells water, food residents' urine and the prevalence of skin lesions in Yatenga province, Burkina Faso. Interdiscipl. Toxicol. 5(1):38-41.

UNICEF (2008). Arsenic Primer Guidance for UNICEF Country Offices on the Investigation and Mitigation of Arsenic Contamination. Water, Environment and Sanitation Section Programme Division UNICEF New York.

Wahed MA, Chowdhury D, Nermell B, Khan SI, Ilias M, Rahman M, Persson LA, Vahter M (2006). A modified routine analysis of arsenic content in drinking-water in Bangladesh by hydride generation-atomic absorption spectrophotometry. J. Health Popul. Nutr. 24(1):36-41.

Welch AH, Westjohn DB, Helsel DR, Wanty RB (2000). Arsenic in ground water of the United States: Occurrence and Geochemistry. Ground water 38(4):589-604.

World Health Organisation (2001). Draft: Abernathy C. and edited by Ann Morgan. Exposure and Health Effects. Office of Water, Office of Science and Technology, Health and Ecological Criteria Division, United States Environmental Protection Agency, Washington, DC, USA. Accessed; www.who.int/water_sanitation_health/dwq/arsenicun3.pdf on 10/09/2012.

academicJournals

Vol. 8(25), pp. 1341-1349, 9 July, 2013
DOI: 10.5897/IJPS2013.3937
ISSN 1992 - 1950 © 2013 Academic Journals
http://www.academicjournals.org/IJPS

International Journal of Physical Sciences

Full Length Research Paper

Design and evaluation of combined solar and biomass dryer for small and medium enterprises for developing countries

Okoroigwe E. C.[1,2]*, Eke M. N.[1] and Ugwu H. U.[3]

[1]Department of Mechanical Engineering, University of Nigeria, Nsukka, Nigeria.
[2]National Centre for Energy Research and Development, University of Nigeria, Nsukka, Nigeria.
[3]Department of Mechanical Engineering, Michael Okpara University of Agriculture, Umudike, Abia State, Nigeria.

Accepted 1 July, 2013

A small scale demonstration model consisting of a combined solar and biomass cabinet dryer with 3 equally spaced drying trays was designed, constructed and evaluated. The results, obtained using fresh yam chips as test material over a four day test period, were satisfactory and useful for optimization purposes. Maximum tray temperature of 53°C was obtained in combination with solar and biomass heating sources even though the ambient temperature for the test period was between 24 and 30°C. An optimal drying rate of 0.0142 kg/hr was achieved with the combined solar and biomass dryer, compared to the lower drying rate of 0.00732 kg/h for the solar drying and 0.0032 kg/h for the biomass drying. This study proved that the efficiency of agricultural dryers could be increased through the use of a combination of solar and biomass heating sources, compared to conventional dryers with only solar or only biomass heating sources. It implies that improvements in the design and construction of the various components of the system would lead to more efficient dryers for use in small and medium business enterprises for sustainable development of developing countries. Using combined solar and biomass dryers have the potential to increase the productivity and resultant economic viability of small and medium-scale enterprises producing and processing agricultural produce in developing countries. African countries, with large quantities of natural resources, like forests and solar radiation, could make the most use of these types of dryers.

Key words: Solar biomass dryer, drying rate, moisture loss, preservation, yam chips, solar radiation, small and medium-scale enterprises.

INTRODUCTION

Although most tropical regions of Africa experience high levels of solar radiation throughout the year, much of this radiation is absorbed by frequent rain and persistent cloud cover. Due to inadequate preservation techniques available to farmers in developing countries, large quantities of agricultural output with high moisture contents are lost annually due to decomposition by micro-organisms. This results in reduction of the net agricultural output and subsequent reduction in the gross domestic product (GDP) of the developing countries.

Dehydration is one of the oldest techniques employed in food or agricultural products storage and preservation (Montero et al., 2010; Montero, 2005; Mujumdar, 2000; Corvalan et al., 1995). The most common method of dehydration is by open air sun drying but this often results in food contamination and nutritional deterioration

*Corresponding author. E-mail: edmund.okoroigwe@unn.edu.ng.

(Ratti and Mujumdar, 1997). Food dehydration technology employs direct and/or indirect mixed mode systems with natural or forced distribution of heated air. According to Madhlopa and Ngwopa (2007), direct heating mode systems consist of direct heating of the items by direct sun radiation through transparent material enclosing the items while indirect heating mode systems consist of heating of air in a separate solar collector and circulating the same through the drying bed where it picks moisture from the crop. The mixed mode drying system combines the features of the two above mentioned systems. The study of solar drying and design of solar dryers are not new but the advent of the renewable energy industry has sparked renewed interest in these fields. There are many sources of literature on solar drying. Ekechukwu (1999) and Ekechukwu and Norton (1999 a, b) have presented overviews of drying principles, theories and solar drying technologies, with a description of low temperature air-heating solar collectors for crop drying applications.

Owing to intermittent solar radiation throughout the day, continuous drying of agricultural products can be accomplished through a combination of solar and non-solar heating sources in a mixed mode system. Thermal storage systems can also be used to increase the efficiency of solar dryers. These thermal storage system range from hybrid modes where, electrical resistances have been used to increase the heating of the air (Prasad and Vijay, 2005; Prasad et al., 2006) to the use of biomass as auxiliary heating source for the drying chamber. Auxiliary heating sources are used to provide uninterrupted supplies of thermal energy for the continuous operation of dryers, during periods of limited solar radiation like night time and cloudy The heated air from the auxiliary heating source passes through pipes or channels and then into the drying chamber via convection. Auxiliary heating source could be powered by electricity or biomass. However, biomass is the most widely used due to its availability and cost effectiveness in rural areas of developing countries. Many solar hybrid dryers have been designed, constructed and tested. Some of these have reached advanced and commercial stages, while some are still undergoing improvements. At the Asian Institute of Technology (AIT), Thailand (Elepaño et al., 2005) a hybrid dryer based on solar and biomass heat sources has been developed and commercialized. This dryer is constructed of bricks and mortar, and is more efficient than a conventional solar cabinet dryer made of steel or aluminum. The dryer has been tested with products such as banana and mushroom. Similarly in Nepal, the Research Centre for Applied Science and Technology (RECAST) developed a similar hybrid dryer based on combined biomass solar drying. These designs were constructed with concrete and bricks. It was capable of drying 10 kg of fresh agricultural products such as radish, carrot, ginger, mushroom, potato and pumpkin.

In Nigeria, some advances have been made in the development of solar hybrid dryers. Danshehu et al. (2008) evaluated a 150 kg kerosene-assisted solar cassava dryer which improved the dehydration process compared to open air solar drying. Similarly, Oparaku et al. (2003) evaluated a solar cabinet dryer with auxiliary heater where appreciable result was obtained. The problems facing the development of this technology in Nigeria include poor design and construction of the dryers, little or no mathematical modeling and poor choice of materials for construction. As a result of these reasons commercial solar dryers are yet to be realized in Nigeria. This has necessitated a search for suitable and efficient dryers based on local technology rather than importing dryers not suited for Nigerian conditions. Nigeria's geography, with tropical forests in the south and high solar radiation levels in the north 3.55 $kWh.m^{-2}.day^{-1}$ (Sambo, 2009), holds great potential for combined solar and biomass drying schemes. Utilising Nigeria's geography and natural resources for solar and biomass drying, could increase the durability and resultant availability and price stability of agricultural and aquatic products throughout the country. It is therefore the objective of this study to design, construct and evaluate the performance of a solar combined with biomass heating dryer for use in developing countries. This preliminary study of the authors utilizes fresh yam chips as test samples in a four day test period.

THEORY

Determination of the heat contribution in drying

The quantity of heat Q_w required, to evaporate moisture of mass m_w is estimated using the basic heat equation.

$$Q_w = m_w L_{vap} \quad (1)$$

where L_{vap} [kJ/kg] is the latent heat of evaporation of water, which can be calculated by the method of Youcef-Ali et al. (2001) as:

$$L_{vap} = 4.186\,(597 - 0.56T_{pr})\ \text{kJ/kg} \quad (2)$$

where T_{pr} [°C] is the product temperature, which can be assumed as the ambient temperature at the coldest weather condition.

$$Q_w = 4.186\, m_w\,(597 - 0.56T_{pr})\ \text{kJ} \quad (3)$$

This represents the heat energy required to dry the items in the dryer to appreciable moisture content status. The sketch below represents the various sources of heat to the drying chambers of the system. Total heat required, Q_w is the sum of the heat which enters the system from the collector, Q_c, the biomass stove, Q_s and the body of the drying chamber, Q_g (Figure 1).

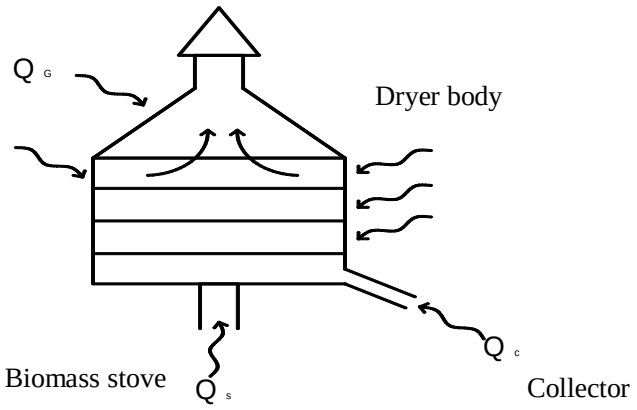

Figure 1. Sketch of the possible heat sources of the dryer.

$$Q_w = Q_c + Q_s + Q_g \quad (4)$$

where the quantity of the heat from the stove, Q_s is the product of the mass of biomass fuel used, m_c and the heating value of the biomass, H_v.

$$Q_s = \eta\, m_c H_v \quad \text{kJ} \quad (5)$$

According to Duffie and Beckman (1991), the useful energy output of a flat plat collector of area A_c is the difference between the absorbed solar radiation and the thermal loss. If I_T is the solar radiation incident on the collector, U_L the overall heat transfer coefficient of the collector and Q_u the heat output of the collector, then,

$$Q_u = A_c[I_T - U_L \Delta T], \quad (6)$$

Where ΔT = T - T_a the difference between the absorber plate temperature and the ambient temperature. Due to difficulty in estimating the absorber temperature because it depends on fluid flow characteristics, it has been suggested that the heat output of the collector be based on the heat removal factor F_R of the collector. But

$$F_R = \frac{m C_p (T_o - T_i)}{A_c[I_T - U_L(T_i - T_a)]} \quad (7)$$

The heat removal factor is a function of the collector efficiency factor F´ which can modify the heat removal factor as

$$F_R = \frac{m C_p}{A_c U_L}\left[1 - \exp\left(-\frac{A_c U_L F'}{m C_p}\right)\right] \quad (8)$$

A graphical representation of the ratio of these factors are provided in Duffie and Beckman (1991) which can be used to estimate the heat removal factor. In order to minimize the heat losses for maximum heat output, it is assumed that both the collector plate and the moving working fluid (air current) should be at the same temperature. Hence the maximum heat output of the absorber plate is

$$Q_u = A_c F_R\,[I_T - U_L(T_i - T_a)] \quad (9)$$

From above this is equivalent to the percentage of the total heat expected from the solar collector to remove m_w of moisture to dry the stuff. The solar radiation component of the Equation 9 can be estimated by the models suggested by Hottel and Wortz (1942) which were improved by Liu and Jordan (1963) as:

$$I_T = I_b R_b + I_d\left(\frac{1+\cos\beta}{2}\right) + I\rho_g\left(\frac{1-\cos\beta}{2}\right) \quad (10)$$

This is the total solar radiation on the tilted surface for 1 h. According to Ulgen (2006) maximum annual energy availability is obtained when the slope of the collector is equal to the angle of latitude of the location for low latitude countries ($\varphi \leq 40^\circ$). Hence, in Nsukka, solar collectors are tilted to the angle of latitude 7°. The heat developed by the direct solar radiation through the transparent body of the dryer can be estimated by the method of Harkness and Mehta (1978) and Okonkwo and Nwoke (2008). This method proposes that the heat developed through the transparent glass material can be estimated by

$$q_c = UA(T_o - T_i) \quad (11)$$

and

$$q_t = (I_D A_s \tau_1 + I_d A \tau_2), \quad (12)$$

Where q_c and q_t are heat transfer by conduction and solar radiation through the glass material respectively. The sum of these components gives the estimated total heat through the glass. From this the total area of the glass (A_s) can be calculated.

MATERIALS AND METHODS

The hybrid solar and biomass dryer (Figure 2) consists of a solar drying section and a biomass stove section. The dryer has the shape of a home cabinet with tilted transparent top, consisting primarily of a drying chamber, biomass stove, and solar collector. The dryer is provided with two heated air inlets: one at the top of the solar collector for the heated air leaving the collector, and the other at the base of the drying chamber for the heated air exiting the biomass stove. The chimney has a height of 180 cm from the ground and is located at the top of the drying chamber and serves as the air outlet. The drying chamber is 59.6 by 59.6 cm in

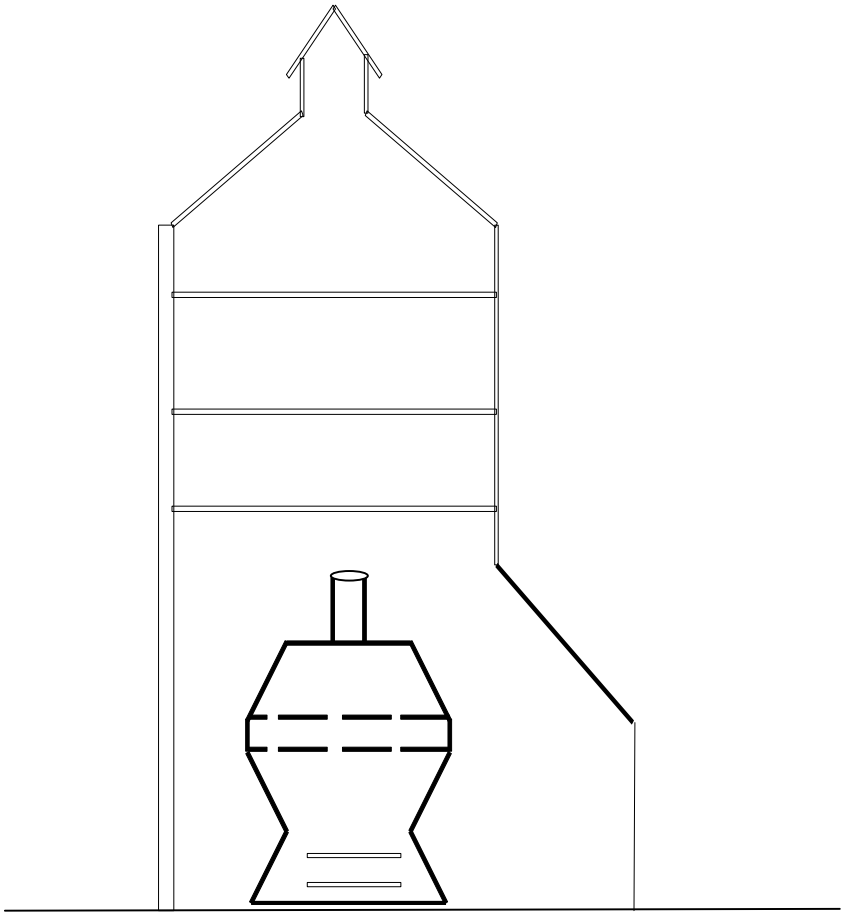

Figure 2. Dimensionless sketch of the combined solar and biomass dryer.

cross-section and has a height of approximately 104 cm. It has three tray levels, and is fitted with a piping system that channels the heat exiting the biomass stove to the different trays.

The biomass stove consists of three main components: the fuel chamber which doubles as the combustion chamber, the primary air inlet and frustum-shaped lid with a little pipe protrusion. The stove is approximately 43 cm in height. The flat plate solar collector of size 0.61× 0.64 m, consists of an absorber, insulation and cover plate. The movement of air from the inlets to the outlets, when the dryer is placed in the path of airflow, brings about a thermo-siphon effect which creates an updraft of solar heated air, which removes moisture from the drying chamber. Ambient air is used as source of air. The performance test of the dryer was carried over a period of four days. The first day consisted of measuring the temperature distribution across the trays of the dryer with no load. The second day consisted of measuring the moisture loss of yam chips on the dryer trays with only solar heating during the day, and then with only biomass heating during the night. The rest of the test period consisted of measuring the moisture loss of the yam chips on the dryer trays with a combination of solar and biomass heating. In all tests yam chips were placed in the open air to dry under direct sunlight as control. The yam chips were prepared from fresh yam purchased from the local market of Nsukka in Nigeria. The chips were washed to ensure that no impurities were involved in the experiment. Equal portions of yam chips of 120 g were weighed out using micro weighing balance and spread in the trays and open sun as control. Temperature changes were monitored using mercury thermometers fixed in the trays while ambient temperature was monitored with k-type thermocouples.

RESULTS AND DISCUSSION

Temperature distribution

The first test was conducted over a period of four hours from 14:00 to 18:00. Figure 3 compares the temperature distributions across the dryer trays over time with no load and with only direct solar radiation as heating source. Within the first hour the temperature of the three trays increased steadily from 38°C (tray 1) to the maximum of 44°C in tray 3. The collector and the transparent glass body performed well as this was reflected in the wide temperature difference between the ambient temperature and the temperature of the trays.

Moisture loss with solar drying

On the second day the system was evaluated with fresh

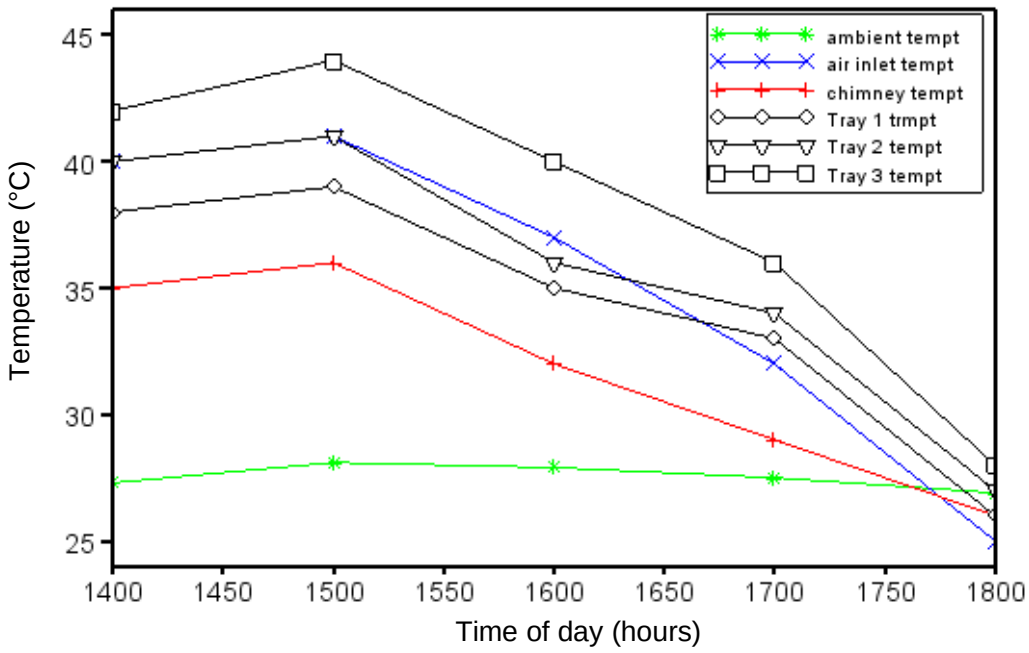

Figure 3. Temperature distribution across the dryer with no load and solar heating only on day one.

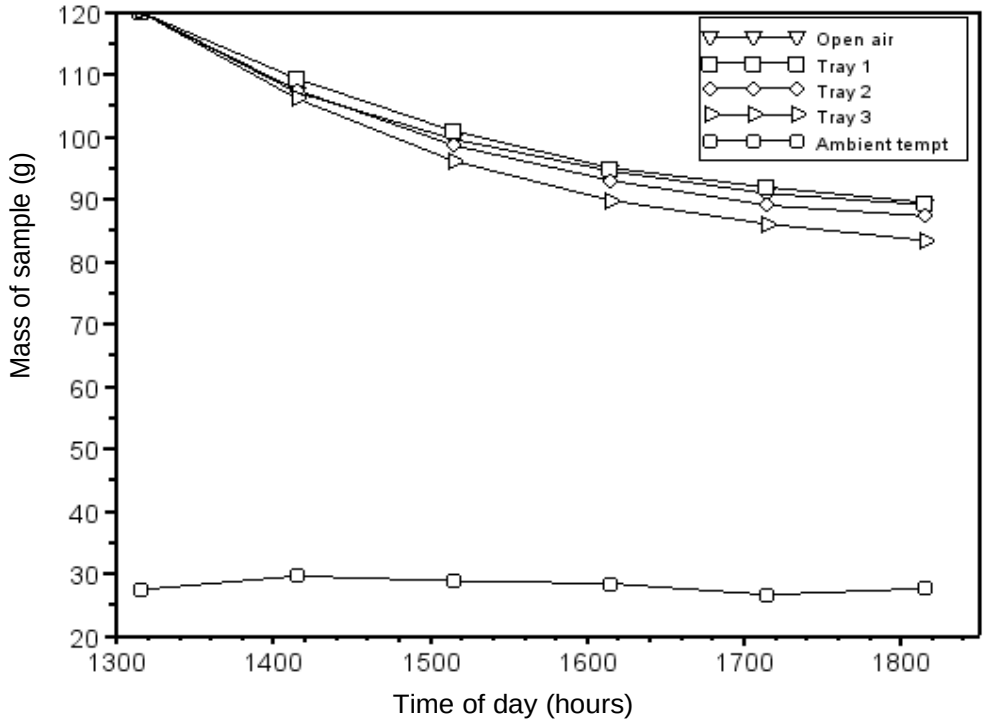

Figure 4. Mass loss of yam chips in the open air compared to yam chips in the dryer with only solar heating on day 2 starting from 13:15.

yam chips whose drying (mass loss) mechanism is shown in Figure 4. A high degree of moisture loss was achieved over the first hour. The mass loss in the open air was greater than in tray 1. This higher drying rate

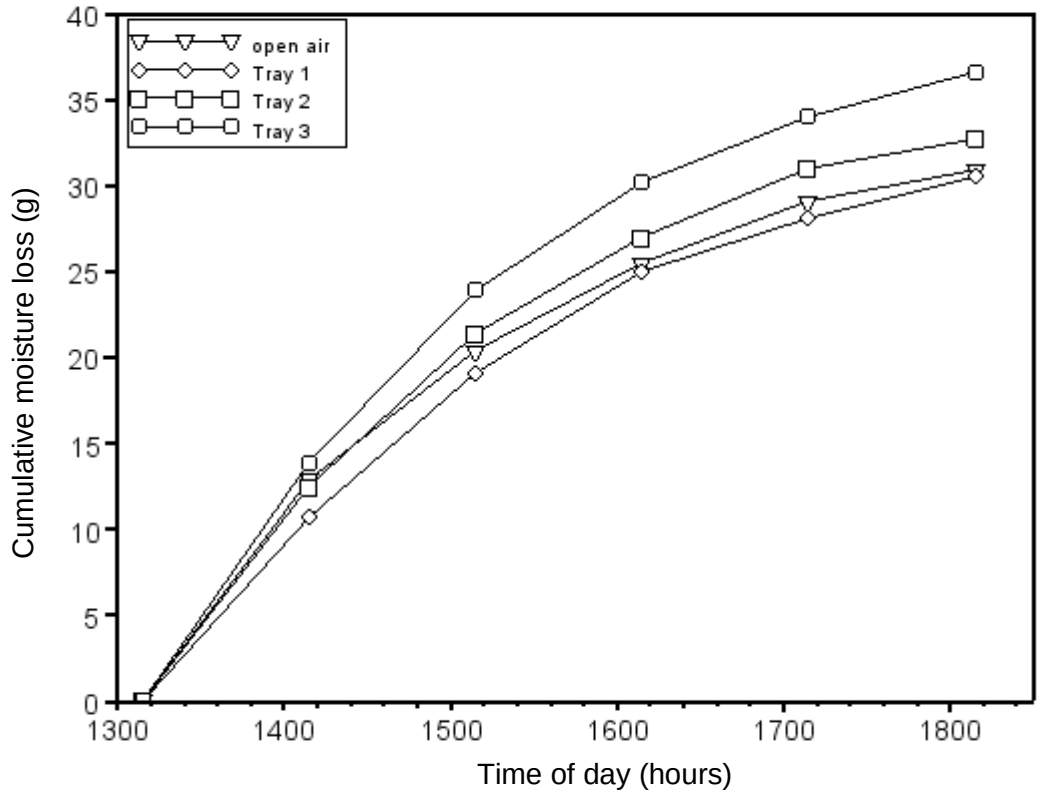

Figure 5. Cumulative moisture loss (removal) with solar drying only.

could have been caused by wind. Surface moisture from the yam chips was lost at a faster rate than its internal moisture, because it takes less energy to evaporate. The rate of total moisture loss slowly reduced after the surface moisture was lost and it took longer to evaporate the internal moisture of the yam chips. The drying effect in the dryer can be observed by the much slower drying rate of the yam chips in the open air compared to the drying rate of yam chips on the dryer trays, until dusk, when the tray temperatures dropped and returned to ambient conditions. The drying rate of 0.00732kg/hr obtained is comparable to 0.009 kg/h obtained by Ajao and Adedeji (2008) using a box type solar dryer for yam drying. The total (cumulative) moisture loss of the yam chips dried in the open air compared to those dried in the solar heated dryer is shown in Figure 5. The cumulative moisture loss in the open air was comparable to the first tray. This could be due to the fact that the first tray did not receive more solar radiation than those dried in the open air, because it was shaded by the upper two trays.

Moisture loss with biomass drying

Figure 6 shows the effect of adding an additional biomass heat source to the drying of the yam chips when solar radiation was not available. The marked moisture loss between 18:00 and 18:30 is expected due to the additional heat source which resulted in increase in temperature of the drying chamber. Within this period, the ambient temperature decreased and there was no sunshine. This implies that additional moisture removal was achieved through the biomass heat addition to the system.

Moisture loss with combined solar and biomass drying

Figures 7 – 9 present the results obtained when biomass was combined with solar drying in the day time. Figure 7 shows the rapid mass loss over the first 30 min while the maximum mass loss of 9.3 g of water occurred after one hour on tray 1. Combining solar heating with additional biomass heating improved the efficiency of the dryer compared to the drying modes where only solar or biomass heating was used. Combining solar and biomass drying reduced the moisture content of the yam chips to 70.83% in 2.5 hours (Figure 7), compared to the moisture content of 75% (Figure 4) of the yam chips with solar drying in 5 hours and 94.44% (Figure 6) in1.25 hours with biomass drying. Comparing this in terms of drying rate, using the tray with the largest cumulative moisture removal, we obtain 0.0142, 0.0032 and 0.00732 kg/h

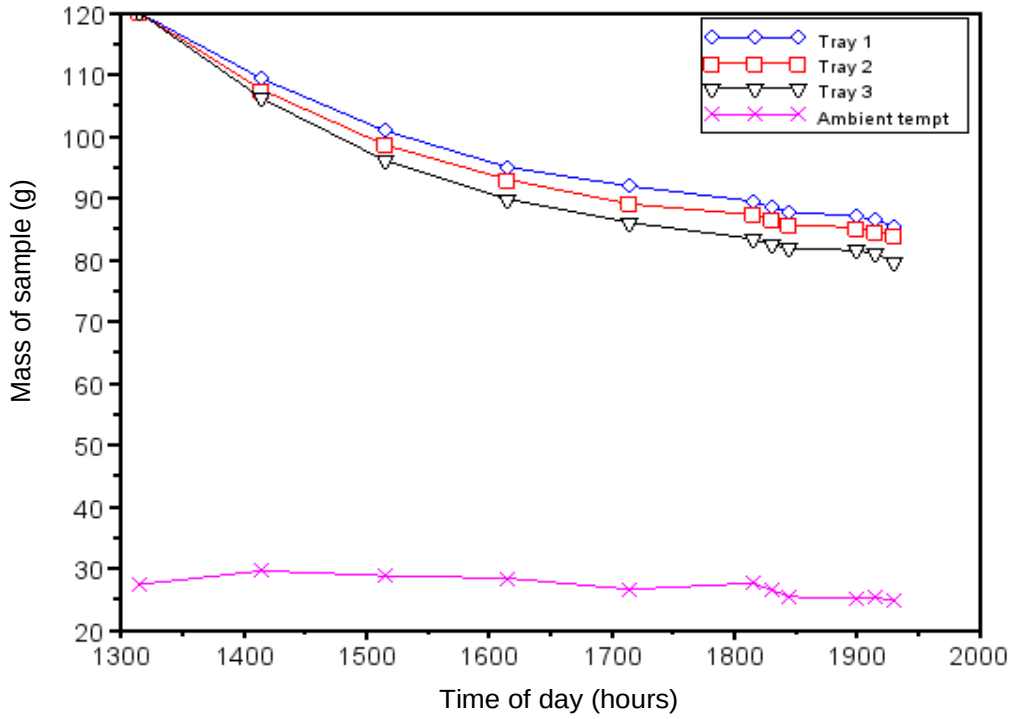

Figure 6. Mass reduction on solar drying in the day and biomass drying in the evening on day 2.

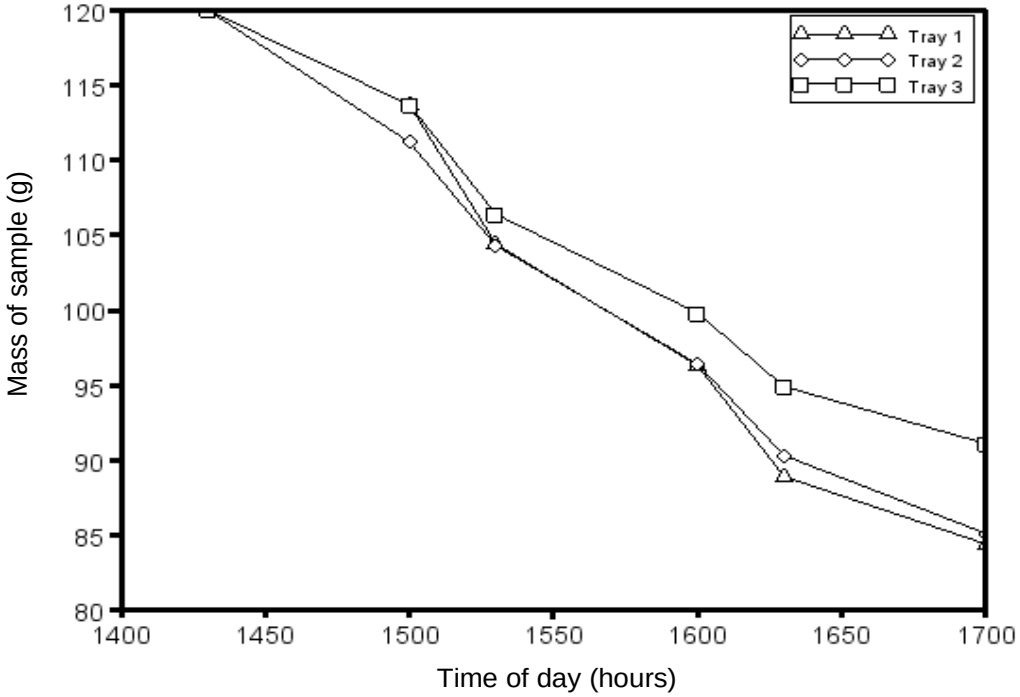

Figure 7. Mass loss with combined biomass and solar drying.

respectively for solar combined with biomass, biomass heating and solar heating only.

Figure 9 also shows that combined solar and biomass heating increased the maximum tray temperature to

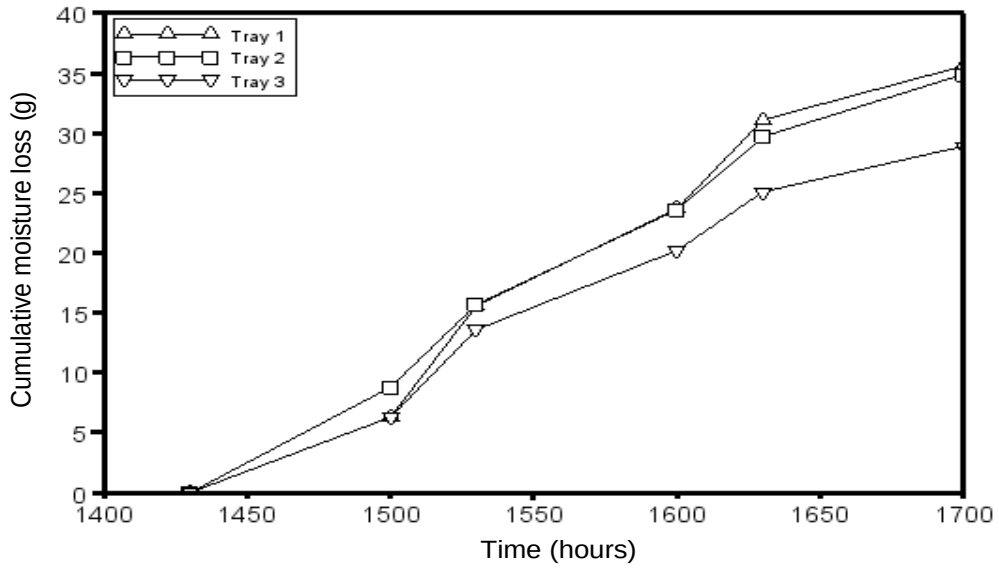

Figure 8. Cumulative moisture loss with combined biomass and solar drying.

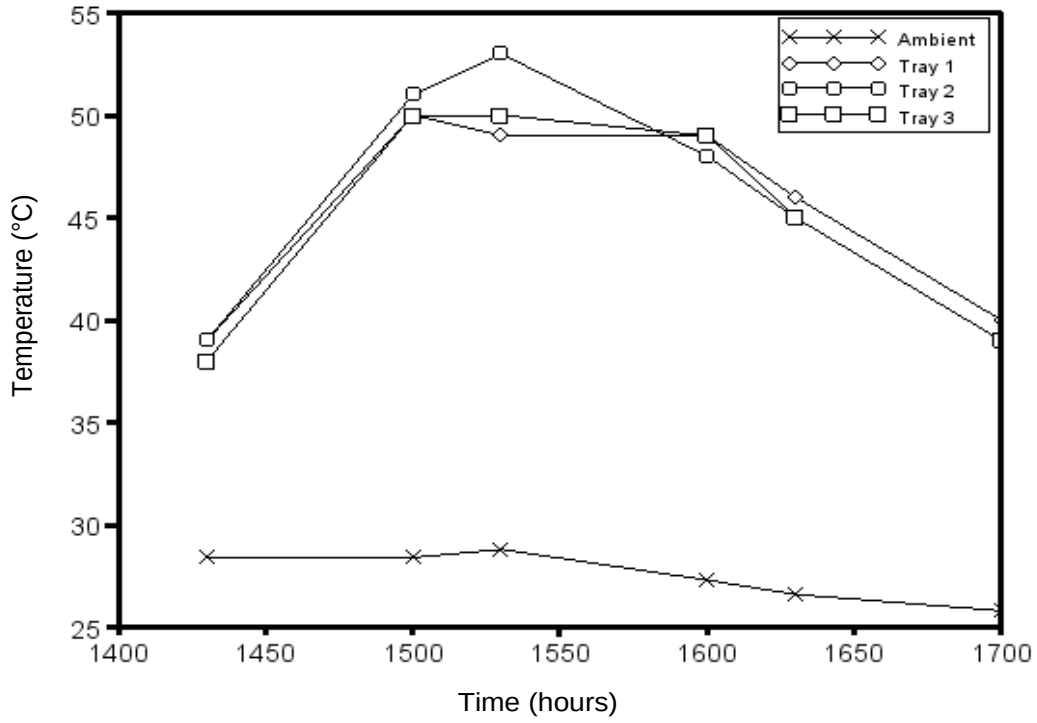

Figure 9. Temperature distribution in the trays with combined biomass and solar drying.

53°C, compared to 44°C with biomass heating and 32°C with solar heating (Figure 3).

Conclusion

This study proved that the efficiency of agricultural dryers could be increased through the use of a combination of solar and biomass heating sources, compared to conventional dryers with only solar or only biomass heating sources. Using combined solar and biomass dryers have the potential to increase the productivity and resultant economic viability of small and medium-scale enterprises producing and processing agricultural

produce in developing countries. Countries, like Nigeria, with large quantities of natural resources, like forests and solar radiation, could make the most use of these types of dryers. It is believed that improvements in the construction of the various components of the system will improve the performance of the dryer for use in small and medium business enterprises.

ACKNOWLEGDMENT

The authors appreciate the suggestions of the reviewers which led to the improvement of different sections of the work

REFERENCES

Ajao KR, Adedeji AA (2008). Assessing some drying rates of some crops in Solar Dryer (Case study: Vegetables, tuber and grain crops). USEP J. Res. info. Civ. Eng. 5(1):1–12.

Corvalan R, Roman R, Saravia L (1995). Engineering of solar drying. CYTED-D, 1995 (in Spanish). IN [Monteroet al 2010].

Danshehu BG, Falayan CO, Chukwuka PC (2008). Performance Evaluation of a 150kg Kerosene Assisted Solar Cassava Dryer. Nig. J. Solar Energy. 19 (2):101-105.

Duffie JA, Bechman WA (1991). Solar Engineering of Thermal Processes. New York: John Wiley and Sons.

Ekechukwu OV, Norton B (1999a). Review of solar-energy drying systems. II: an overview of solar drying technology. Energy Convers. Manage. 40(6):615–655.

Ekechukwu OV, Norton B (1999b). Review of solar-energy drying systems. III: low temperature air-heating solar collectors for crop drying applications. Energy Convers. Manage. 40(6):657–667.

Ekechukwu OV (1999). Review of solar-energy drying systems. I: an overview of drying principles and theory. Energy Convers. Manage. 40(6):593–613.

Elepaño RA, Del Mundo RR, Gewali BM, Sackona P (2005). Technology Packages: Solar, Biomass and Hybrid Dryers. Regional Energy Resources Information Center, RERIC. pp. 2–18.

Harkness EL, Mehta ML (1978). Solar Radiation. Solar Radiation Control in Buildings. Applied Science Pubblishers. In [Okonkwo and Nwoke 2008] P. 102.

Hottel HC, Woertz BB (1942). Performance of Flat Plate Solar Heat Collectors. Transactions of ASME 64(91), 1942. In [Duffie and Bechman 1991].

Liu BY, Jordan RC (1963). The long Term Average Performance of Flat plate Solar Energy Collectors Solar Energy 7(53). In [Duffie and Bechman 1991].

Madhlopa A, Ngwalo G (2007). Solar dryer with thermal storage and biomass-backup heater. Solar Energy 81:449–462.

Montero I (2005). Modeling and construction of hybrid solar dryer for biomass byproducts. PhD thesis, Department of Chemical and Energetics Engineering, University of Extremadura, 2005. (in Spanish). In [Montero et al 2010] P. 286.

Montero I, Blanco J, Miranda T, Rojas S, Celma AR (2010). Design, construction and performance testing of a solar dryer for agro-industrial by-products. Energy Convers. Manage. 51:1510–1521.

Mujumdar AS (2000). Drying technology in agriculture and food sciences. Enfield – NH, USA: Science Publishers, Inc.; 2000. IN [Montero et al 2010].

Okonkwo WI, Nwoke OO (2008). Family Size Green House Solar Energy Crop Dryer. Nig. J. Solar Energy 19(2):6–10.

Oparaku NF, Unachukwu GO, Okeke CE (2003). Design, Construction and Performance evaluation of Solar Cabinet Dryer with auxiliary heater. Nig. J. Solar Energy. 14:41–50.

Prasad J, Vijay VK, Tiwari GN, Sorayan VPS (2006). Study on performance evaluation of hybrid drier for turmeric (Curcuma longa L.) drying at village scale. J. Food Eng. 75(4):497–502. In [Montero et al. 2010].

Prasad J, Vijay VK (2005). Experimental studies on drying of Zingiber officinale, Curcuma longa I and Tinospora cordifolia in solar–biomass hybrid drier. Renew Energy 30(14):2097–109. In [Montero et al. 2010].

Ratti C, Mujumdar AS (1997). Solar dryer of foods: modeling and numerical simulation. Solar Energy. 60:151–157.

Sambo AS (2009). Strategic Developments In Renewable Energy In Nigeria. International Association for Energy Economics Third Quarter 2009 pp.15–19. www.iaee.org/en/publications/newsletterdl.aspx?id=7 *assessed6/9/2012*

Ulgen K (2006). Optimum Tilt Angle for Solar Collectors. Energy Sources, Part A, 28:1171–1180.

Youcef-Ali S, Messaoudi H, Desmons JY, Abene A, Le Ray M (2001). Determination of the Average Coefficient of Internal Moisture Transfer during the Drying of a Thin Bed of Potato Slices. J. Food Eng. 48(2):95-101.

academicJournals

Vol. 8(25), pp. 1350-1361, 9 July, 2013
DOI: 10.5897/IJPS2013.3951
ISSN 1992 - 1950 © 2013 Academic Journals
http://www.academicjournals.org/IJPS

International Journal of Physical Sciences

Full Length Research Paper

Geoelectrical evaluation of groundwater potentials of Bwari basement area, Central Nigeria

A. E. Adeniji[1]*, D. N. Obiora[1], O. V. Omonona[2] and R. Ayuba[3]

[1]Department of Physics and Astronomy, University of Nigeria, Nsukka, Nigeria.
[2]Department of Geology, University of Nigeria, Nsukka, Nigeria.
[3]Department of Earth Sciences, Kogi State University, Anyigba, Nigeria.

Accepted 1 July, 2013

An investigation has been made of the groundwater potentials of Bwari basement area using solely geoelectric surveys. Twenty vertical electrical soundings along different transverses were conducted with maximum electrode spacing of 300 m. The results revealed that the area is characterized with 3 to 6 geoelectric subsurface layers with variability in resistivities and thicknesses of the different layers. The overburden thickness ranged from 6.9 to 72.9 m, with thinnest and thickest overburden observed at the central and western areas respectively. Dar Zarouk parameters (transverse resistance and coefficient of anisotropy), reflection coefficient, resistivity contrast, weathered layer thickness and overburden thickness were used as indices for evaluation of groundwater potentials. The area's groundwater productivity potential was hence, classified into two zones namely; high and low. This study has revealed that no single factor (index) determines the groundwater productivity potential but a combination of two or more factors. For example, not all the areas with thick overburden or high weathered layer thickness correspond to high groundwater potential.

Key words: Groundwater potential, electrical resistivity, transverse resistance, coefficient of anisotropy, Bwari.

INTRODUCTION

Water is essential to the continuous existence of man. Sources of water supply in Bwari range from pipe borne water (tap water), borehole, open hand dug well and stream. Tap water and borehole which constitute 9 and 23% of total water supply in the area are known to be the only sources of potable water for drinking and domestic purposes (MDG, 2012). Access to potable water supply over the years has been declining due to influx of people into the area without a corresponding expansion in the pipe borne water supply and borehole drilling programmes. Most of the water supply facilities (pipe borne water and boreholes) are fairly functional to non-functional, and this could be attributed to the use of substandard materials and wrong sitting of boreholes (MDG, 2012).

Electrical resistivity survey, a geophysical survey technique has proved to be an effective and a reliable tool in locating viable aquifers for continuous and regular water supply (Todd and Mays, 2005). This method has the advantage of non-destructive effect on the environment, cost effective, rapid and quick survey time and less ambiguity interpretations of results when compared to other geophysical survey methods (Todd, 1980). Twenty vertical electrical resistivity soundings along different transverses have therefore been carried out with the aim of delineating areas or zones of high and low groundwater potentials which is intended to aid in the groundwater planning and development of the area.

*Corresponding author. E-mail: emmaabidec@yahoo.com.

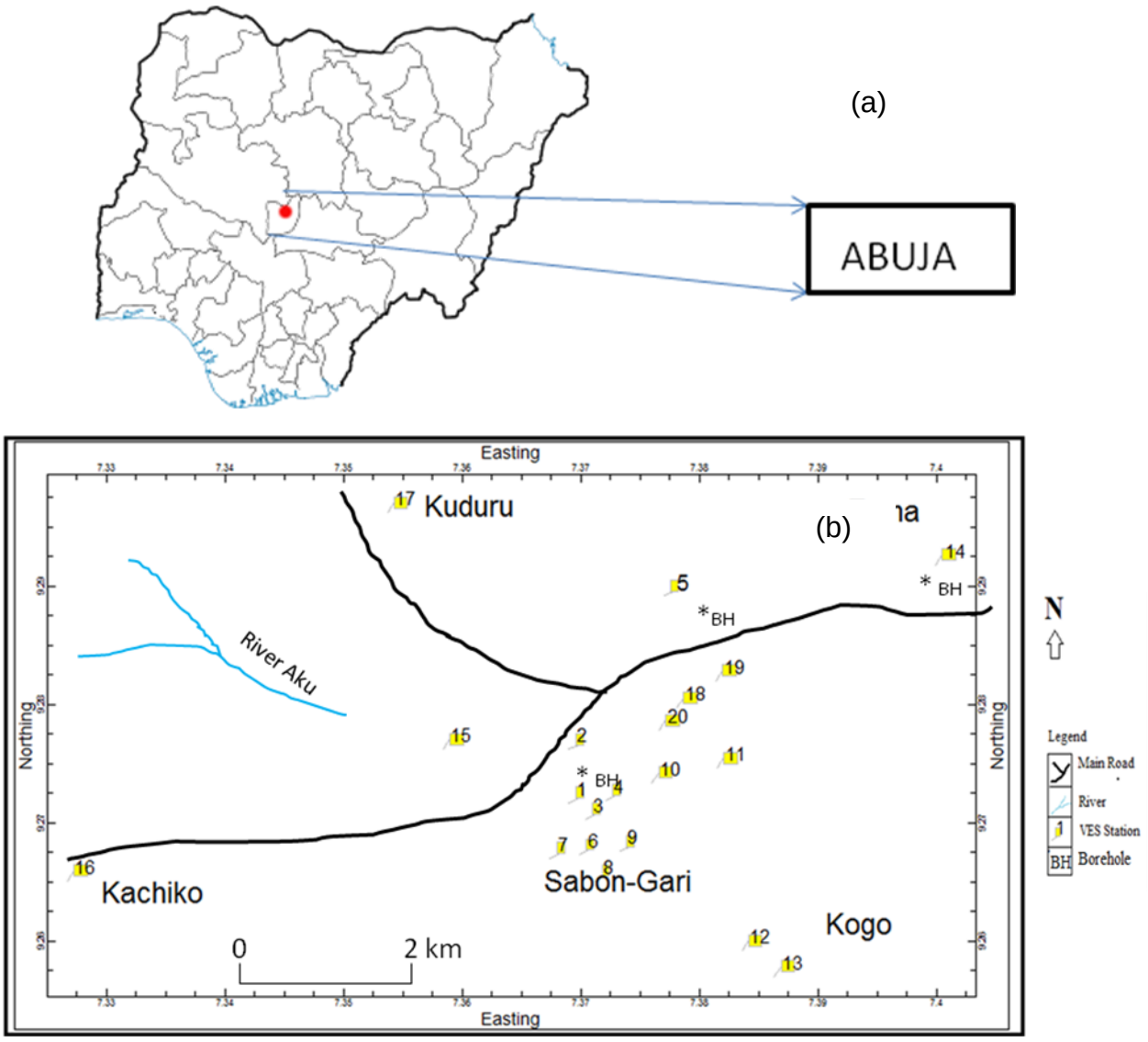

Figure 1. (a) Shows the map of Nigeria in which the study area is located. (b) Location and VES station map of the study area.

Study area

The study area is Bwari located in Abuja, Nigeria between latitudes 9° 15'N and 9° 18'N and longitudes 7° 19'E and 7° 25'E (Figure 1). It covers an approximate area of about 40 km^2. It is bounded in the north by Kaduna state, in the south by the FCT municipal town, in the East by Nassarawa state and in the west by Niger state. The general elevation of the study area varies considerably; it ranges from 535 to 597 m above mean sea level. The climate of the area is made up of two distinct seasons; the dry and rainy seasons. The dry season usually lasts from November to February with warm sunshine and hazy harmattan around December to January. The rainy season lasts from April to October. Mean annual rainfall ranges from 1500 to 2099 mm while the mean annual temperature varied from 27 to 30°C. The area falls under the Guinea savannah vegetation and is drained mainly by River Iku and its tributaries.

The study area is underlain by PreCambrian crystalline rocks of the Basement Complex. Rahaman (1989) classified the Basement Complex rocks of Nigeria into five groups namely; (i) Migmatite-Gneiss-Quarzite Complex which comprises of migmatite, gneisses, quartzite and quartz schist and small lenses of calcilicate rocks, (ii) Slightly migmatised to unmigmatised paraschist and meta-igneous rocks. (iii) Charnockitic rocks, (iv) Older granites which comprises of rock varying in composition from granodiorite to granite and potassic syenite, (v) Unmetamorphosed doleritc dykes. The Bwari

is underlain by rocks of the Precambrian basement complex of north central Nigeria. The lithological units include the migmatite-gneiss complex and granitoids, (Mabogunje, 1977). The migmatite-gneiss complexes form generally the ridges and the icebergs while the granitiods form lowland outcrops with coarse texture. The study area can be divided into two hydro-geological units namely: the aquiferous zone within the weathered overburden overlying the basement rocks and the aquiferous zone within the intense fracture joint system in the partially weathered basement.

MATERIALS AND METHODS

This work has utilized the electrical resistivity survey method in delineating the groundwater potential of the study area, twenty vertical electrical soundings were carried out and the ALLIED OHMEGA SAS 300B model Terrameter and its accessories were used. The conventional Schlumberger array pattern, with half electrode spacing (AB/2) varying from 1 m to a maximum of 150 m was adopted. The apparent resistivity was computed using equation:

$$\rho_a = \frac{\pi L^2}{2l} R = GR \ , \tag{1}$$

where

ρ_a is apparent resistivity

π is $\frac{22}{7}$

$G = \frac{\pi L^2}{2l}$ is geometrical factor

$R = \frac{\Delta V}{I}.$ is the resistance

$L = \frac{AB}{2}$ is the half the current electrodes separation, and

$l = \frac{MN}{2}$ is the half the potential electrode separation.

The apparent resistivity values obtained from Equation (1) were plotted on bi-log graph against the half current electrode separation spacing. From these plots, qualitative deductions such as the resistivity of the first or top layer, the depth of each layer and the curve signatures or types were made. The initial quantitative interpretations were made using partial curve matching technique in which the field curves produced or generated were matched segment by segment with the appropriate master curves and auxiliary curves.

The resistivities and thicknesses of the various layers were improved upon by employing an automatic iterative computer program following the main ideas of Zohdy and Martin (1993). The WINRESIST computer software was employed for carrying out the iteration and inversion processes. Each iteration process was conducted for each sounding station until the root mean square (RMS) error of lower than 5% was obtained. The secondary parameters (longitudinal conductance (S_i), transverse resistance (T_i), longitudinal resistivity (ρ_L), transverse resistivity (ρ_l) and coefficient of anisotropy (λ)) were determined from the layers' resistivities and thicknesses using the mathematical relations (Zohdy et al., 1974):

$$S_i = \sum_{i=1} \frac{h_i}{\rho_i} \tag{2}$$

$$T_i = \sum_{i=1} h_i \rho_i \tag{3}$$

$$\rho_L = \sum_{i=1} \frac{h_i}{S_i} \tag{4}$$

$$\rho_l = \sum_{i=1} \frac{T_i}{h_i} \tag{5}$$

$$\lambda = \sqrt{\frac{\rho_l}{\rho_L}} \tag{6}$$

The reflection coefficients (R_C) and fracture contrast (F_C) of the fresh basement rock of the study area were calculated using the method of Olayinka (1996); Bhattacharya and Patra (1968) and Loke (1999):

$$R_C = \frac{\rho_n - \rho_{n-1}}{\rho_n + \rho_{n-1}} \tag{7}$$

$$F_C = \frac{\rho_n}{\rho_{n-1}} \tag{8}$$

Where, ρ_n is the layer resistivity of the nth layer and ρ_{n-1} is the layer resistivity overlying the nth layer.

RESULTS AND DISCUSSION

Geoelectrical characteristics

The summary of the interpreted electrical resistivity survey is presented in Table 1. The geoelectric section (Figure 2a and b) reveals that the area is characterized by 3- to 6-geoelectric subsurface layers. Eight transverses connecting the twenty VES points were covered and their subsurface geo-electric sections are presented in figure 2. From the figure, the geo-electric subsurface section ranged from 3 to 6 layers with 4-layer type occurring more. The 3-layer geoelectric section is characterized by H curve type (Figure 3) and is generally made up of top loose soil, laterite/clay and fresh basement rock from top to bottom with variable

Table 1. Layers' resistivity, thicknesses and curve types.

VES station	Layer Resistivity (ohms)* ρ_1	ρ_2	ρ_3	ρ_4	ρ_5	ρ_6	h_1	Layer thickness (m)+ h_2	h_3	h_4	h_5	Curve type
1	442	5078	1982	62	234	21063	2.6	0.4	5.4	15.9	48.6	AKH
2	44	2184	35	1668			2.1	0.8	25.5			KH
3	349	18	3357				2.9	6.3				H
4	214	62	1226				5.6	52.2				H
5	1177	155	7040				6.6	37.5				H
6	479	1047	1560	10618			1.3	6.5	18.6			AA
7	251	1066	2107	134	5338		1.6	1.3	4.0	25.6		AKH
8	344	274	5117	54677			1.1	11.9	1.0			HA
9	336	43	909				1.1	5.8				H
10	207	64	5941				1.0	9.3				H
11	110	59	3257	16	1232		1.5	1.5	1.0	6.2		HKH
12	455	482	111	6391			4.8	3.9	30.5			KH
13	438	11908	575	25454			1.5	0.7	63.7			KH
14	1109	357	6830	92805			1.4	22.6	1.9			HA
15	278	588	75	7075			1.6	1.4	54.9			KH
16	387	562	97	413			2.2	0.8	11.0			KH
17	212	314	77	17627			1.7	0.6	6.2			KH
18	95	101	13242				3.5	4.1				H
19	495	772	305	1391			3.5	0.9	15.9			KH
20	496	942	207	756			6.1	0.2	26.5			KH

VES-vertical electrical sounding; ρ -layer resistivity; h-layer thickness, m-meter.

thicknesses and resistivities. The 4-layer geoelectric section is characterized by KH and HA curve types (Figures 4, 5 and 6). The 5-layer geoelectric section is characterized by AKH and HKH curve types (Figures 7 and 8) and the six layer characterized by AKH curve types (Figure 8). Vertical electrical sounding (VES) stations 2, 5 and 14 were carried out in the vicinity of existing boreholes. The inferred lithologies and thicknesses of the various layers from the subsurface geoelectric sections of these VES stations were compared with the lithologic logs of the boreholes located very close to them and it was revealed that they are very well correlated (Figure 9). The topsoil layer is made up of loose sand, sandy clay, clay and lateritic soil and its thickness and resistivity varied from 1.0 to 6.6 m, with a mean of 2.78636m and from 44.0 to 1177 Ωm, with a mean of 415.4091 Ωm respectively. Underlying the topsoil layer is the weathered layer. The weathered layer thickness and resistivity range between 1.0 and 63.7 m with a mean of 20.675 m and from 35 to 13242 Ωm, with a mean of 3060.318 Ωm respectively. The partially weathered/fractured layer where found underlies the weathered layer and resistivity of this layer range from 16 to 92805 Ωm, with a mean of 19494.25 Ωm and where it occurs as the last layer from the surface, it has an infinite thickness. This layer together with the weathered layer constitutes the aquiferous units where they have appreciable thicknesses in the basement area. Overburden thickness measured varies from 6.9 to 72.9 m, with a mean of 21.5 m.

Evaluation of groundwater potentials

The groundwater potentials of the area are evaluated based on the following indices; weathered layer thickness and resisitivity, overburden thickness, transverse resistance, coefficient of anisotropy, reflection coefficient and resistivity contrast. The weathered/or weathered fractured layer constitute the water saturation zone or aquifereous units. Areas where weathered layer thickness is greater than 25 m (Table 2) and of low clay content as indicated by the resistivity (> 150 Ωm) value is categorized to be area of high groundwater potentials. The spatial distribution of the weathered layer is presented in Figure 10. From the figure, area around VES stations 12, 13 and 15 have very high (in the range of 40 to 65 m) weathered layer thickness while area around VES stations 8, 9, 11 14, 16, 17 and19 have very low (in the range of 5 to 15 m) weathered layer thickness. Zones that have thick overburden and low percentage of

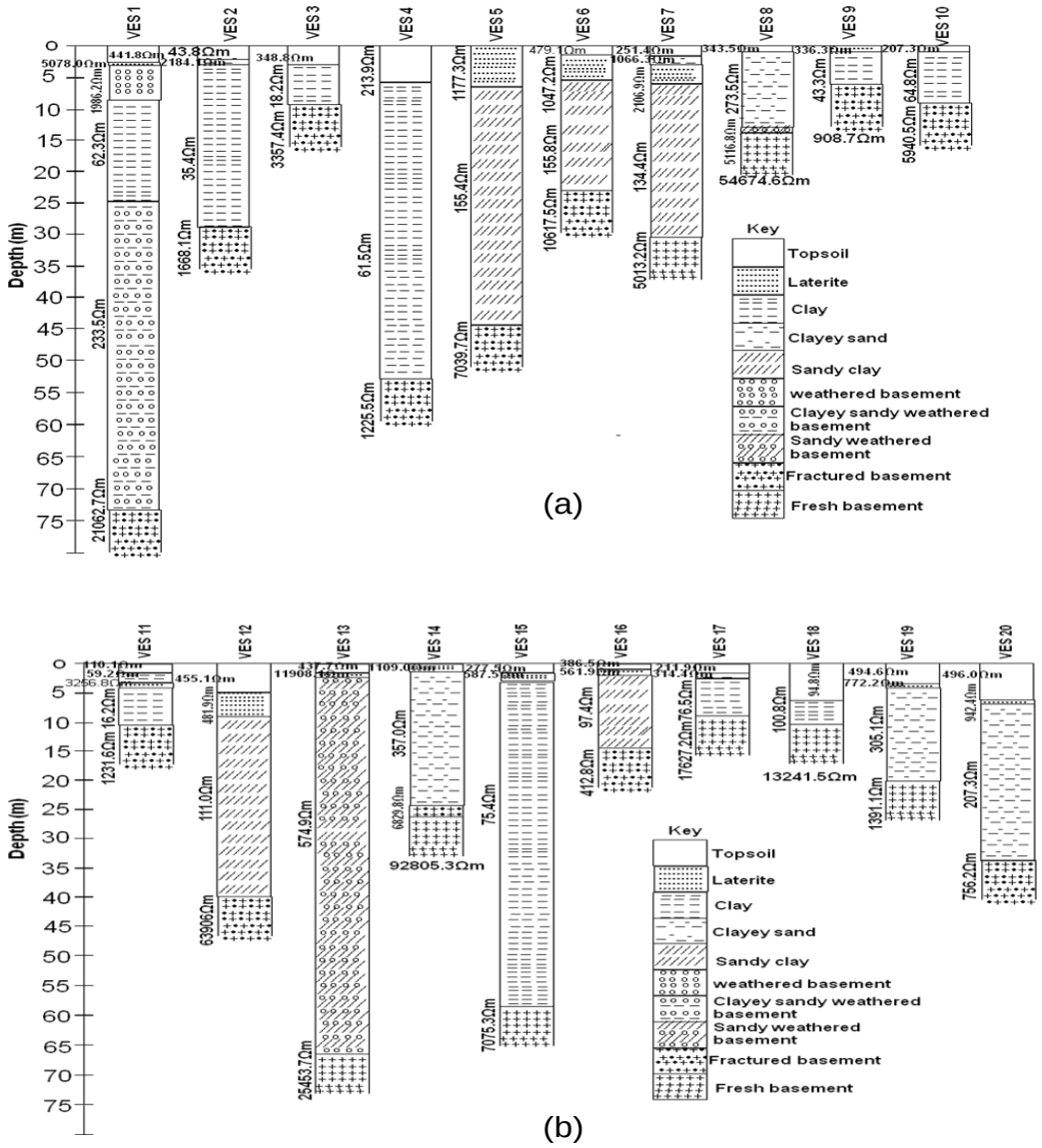

Figure 2. (a) 1-D geoelectrical models for VES 1 – 10, (b) 1-D geoelectrical models for VES 11 – 20.

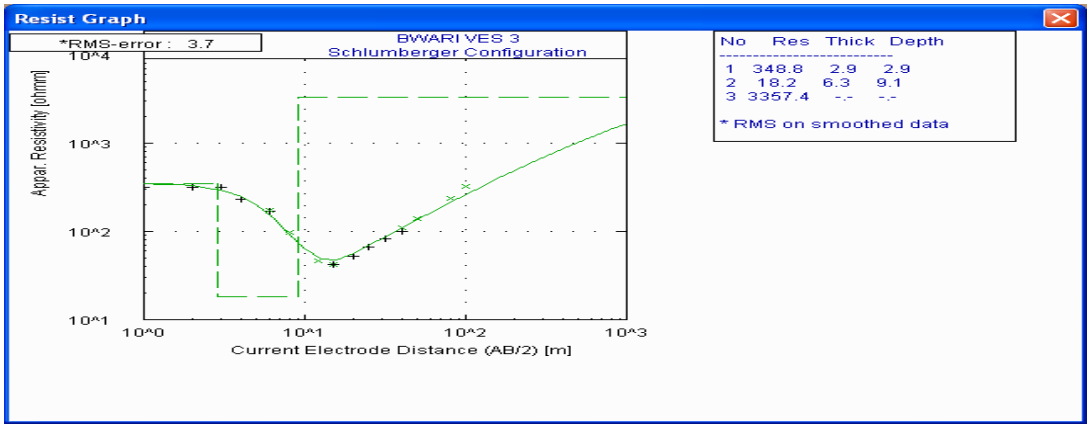

Figure 3. Typical H curve type.

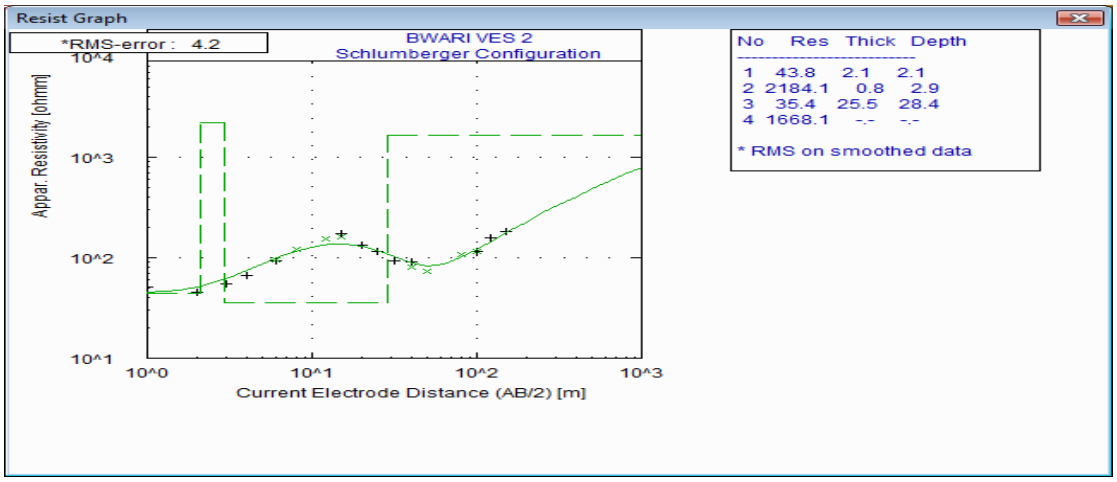

Figure 4. Typical KH curve type.

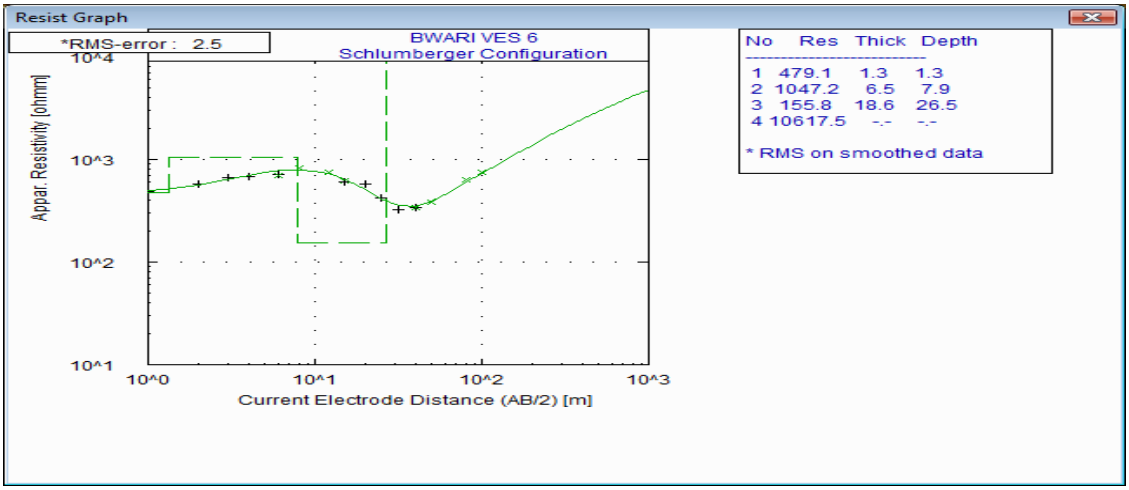

Figure 5. Typical KH curve type.

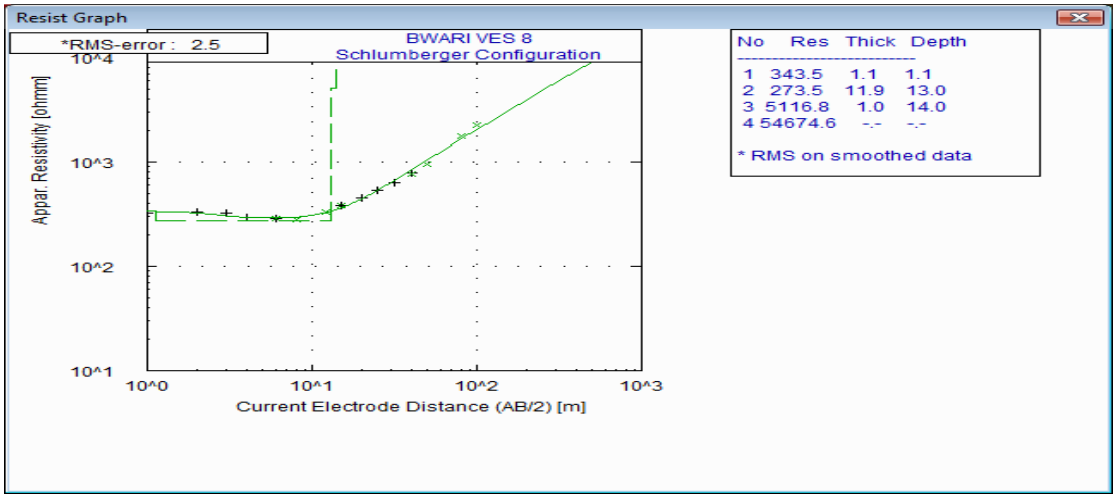

Figure 6. Typical HA curve type.

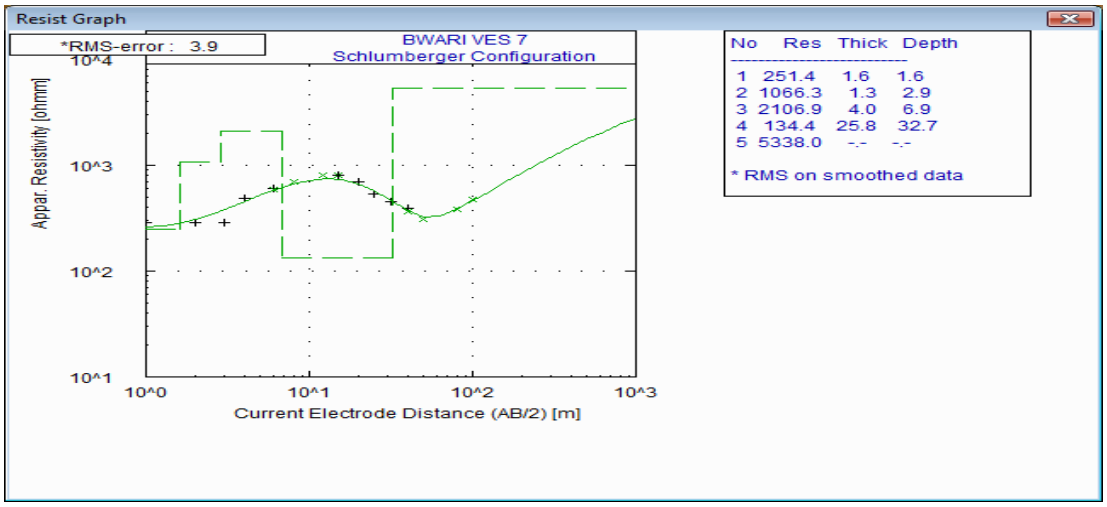

Figure 7. Typical AKH curve type.

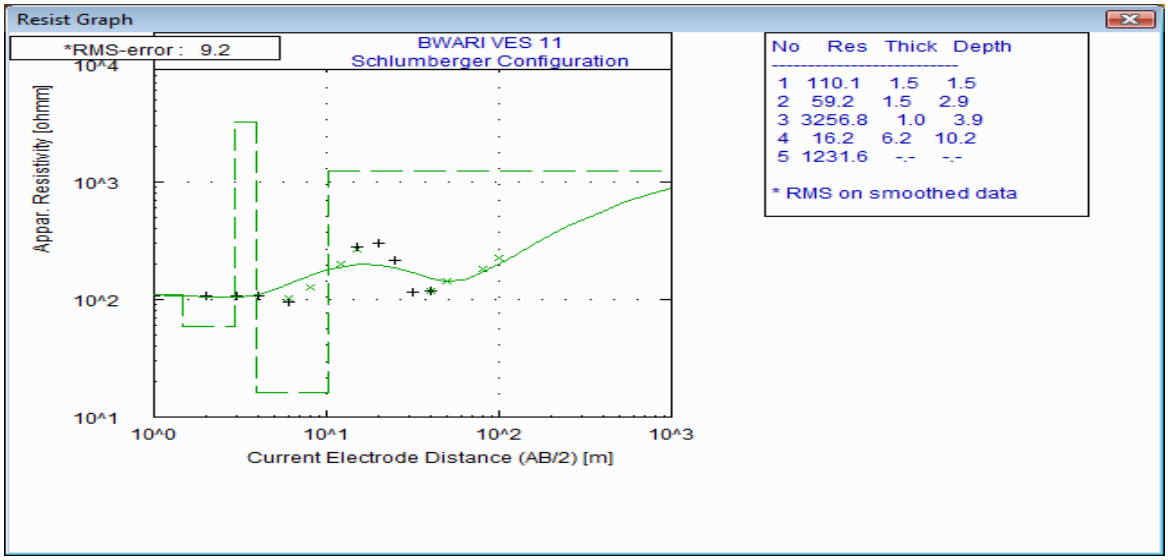

Figure 8. Typical HKH curve type.

clay in which intergranular flow is dominant are known to have high groundwater potential particularly in basement complex terrain (Okhue and Olorunfemi, 1991). In this study, areas with overburden thickness greater than 30 m such as areas around VES stations 2, 12, 13 and 15 (Figure 11) are classified as high groundwater potential zones. Transverse resistance (T_i) has a direct relation with transmissivity (T) and the highest T_i values reflect most likely the highest T values of the aquifers or aquiferous units and vice-versa (Anudu et al., 2011; Kumar et al., 2001). Vertical electrical sounding stations such as 6, 9, 12, 13 and 14 with computed transverse resistance greater than 5000 Ωm^2 (Figure 12) are defined as areas of high groundwater potentials.

Generally, the co-efficient of the anisotropy is 1 and does not exceed 2 in most of the geological conditions (Zohdy et al., 1974). Compact rock at shallow depth increases the coefficient of the anisotropy (Keller and Frischknecht, 1966). Hence, these areas can be associated with low porosity and permeability. The areas with 1.0 and less than 1.5 anisotropy (VES stations 2, 12, and 16; Figure 13) values (high porosity and permeability) are considered as high groundwater potential zones (Rao et al., 2003). The reflection coefficient and resisitivity contrast at fresh basement rock interface can provide some insight into the aquiferous nature of the basement rocks. According to Olayinka (1996), he observed that area of lower reflection

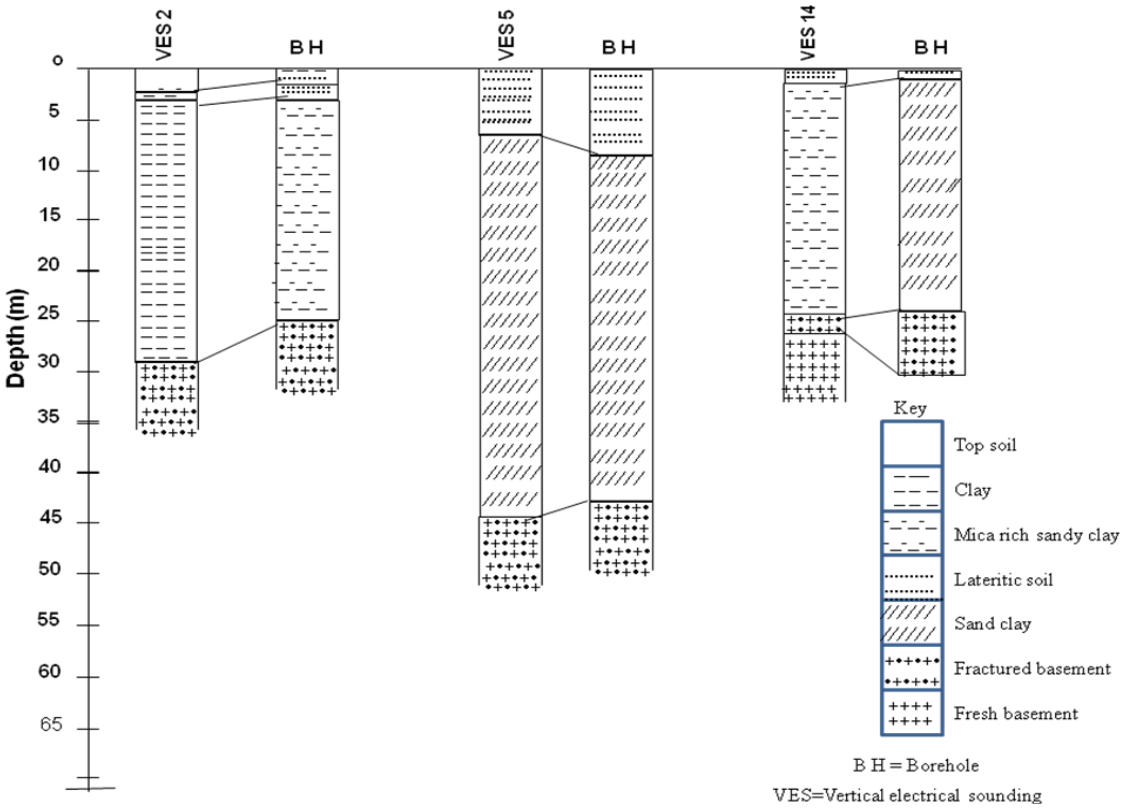

Figure 9. Correlation between geoelectric section and lithological logs.

Table 2. Groundwater potential indices

VES station	Weathered layer thickness (m)	Overburden thickness(m)	Transverse Resistance (Ωm^2)	Coefficient of Anisotropy	Reflection coefficient	Resistivity contrast
1	48.6	72.9	25095.35	0.8159	0.97	90.65
2	25.5	28.4	2741.96	0.6186	0.96	46.66
3	6.3	9.2	1126.18	1.421	0.99	186.50
4	46.6	57.8	4063.74	0.8755	0.90	19.77
5	37.5	44.1	13597.68	1.0558	0.96	45.42
6	25.1	26.4	10327.51	0.7280	0.74	6.80
7	25.8	32.5	8134.96	0.8108	0.95	39.88
8	1.0	14.0	8749.3	0.6911	0.83	10.69
9	5.8	6.9	620.74	0.7476	0.91	21.14
10	9.3	10.3	809.94	0.9397	0.98	92.82
11	7.2	10.2	3611.19	0.2613	0.97	77.00
12	30.5	39.2	7449.39	1.3469	0.97	57.58
13	63.7	65.9	45613.35	1.2117	0.96	44.27
14	1.9	25.9	22597.42	0.4973	0.86	13.59
15	54.9	57.9	5405.96	2.7006	0.98	94.33
16	12.3	14.0	2202.61	1.0102	0.62	4.26
17	6.2	8.5	1023.17	0.9419	0.99	228.90
18	4.1	7.6	745.08	0.9995	0.98	131.11
19	15.7	20.3	7216.15	0.9678	0.64	4.56
20	26.7	32.8	8707.53	0.9383	0.57	3.65

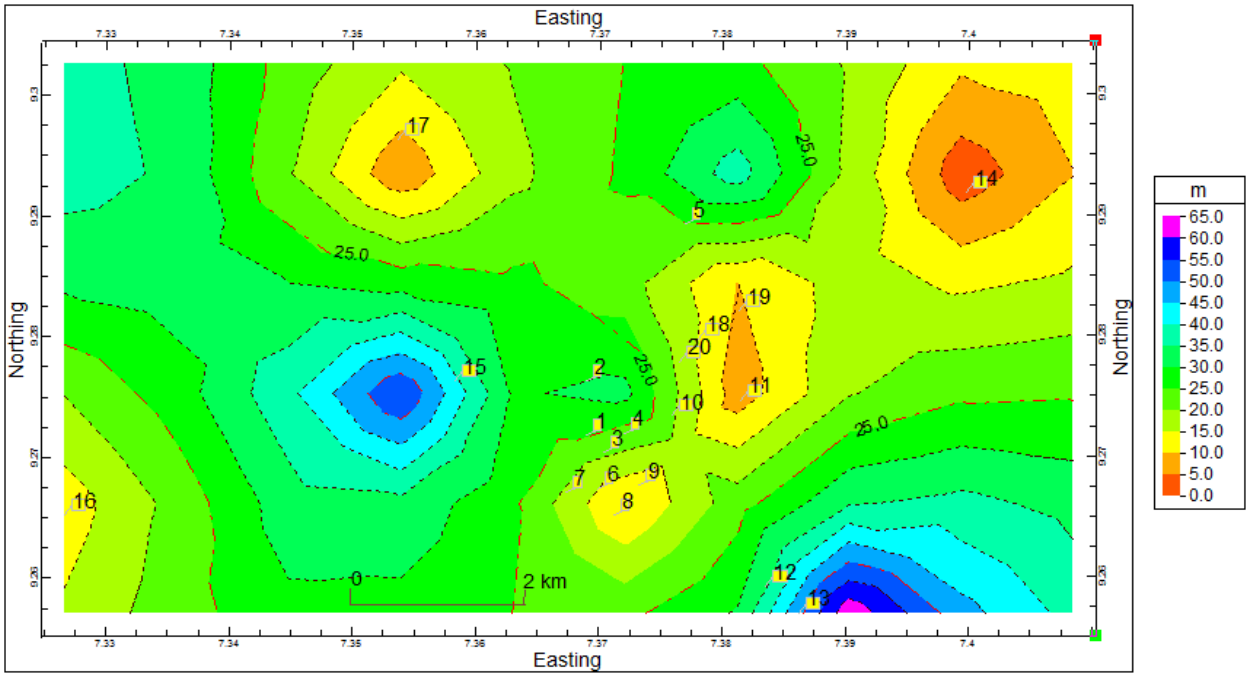

Figure 10. Spatial distribution of weathered layer thickness of the study area.

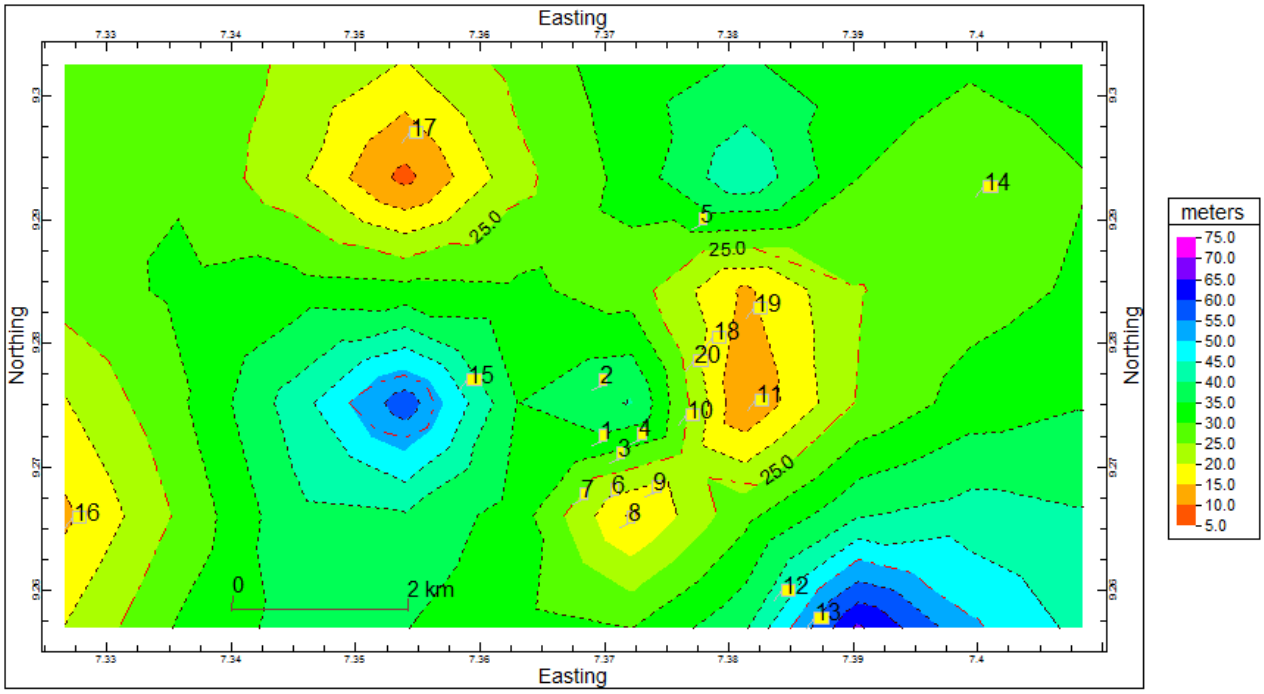

Figure 11. Spatial distribution of overburden thickness of the study area.

coefficient value exhibits a fracture of the basement rock, and hence, has a higher water potential. In the present study, reflection coefficient and resistivity contrast values less than 0.9 and 19 (VES stations such as 14 and 16; Figures 14 and 15) respectively may be indicative of high density water filled fracture (Anudu et al., 2011; Olayinka et al., 2000). The groundwater potentials map of the area is presented in Figure 16.

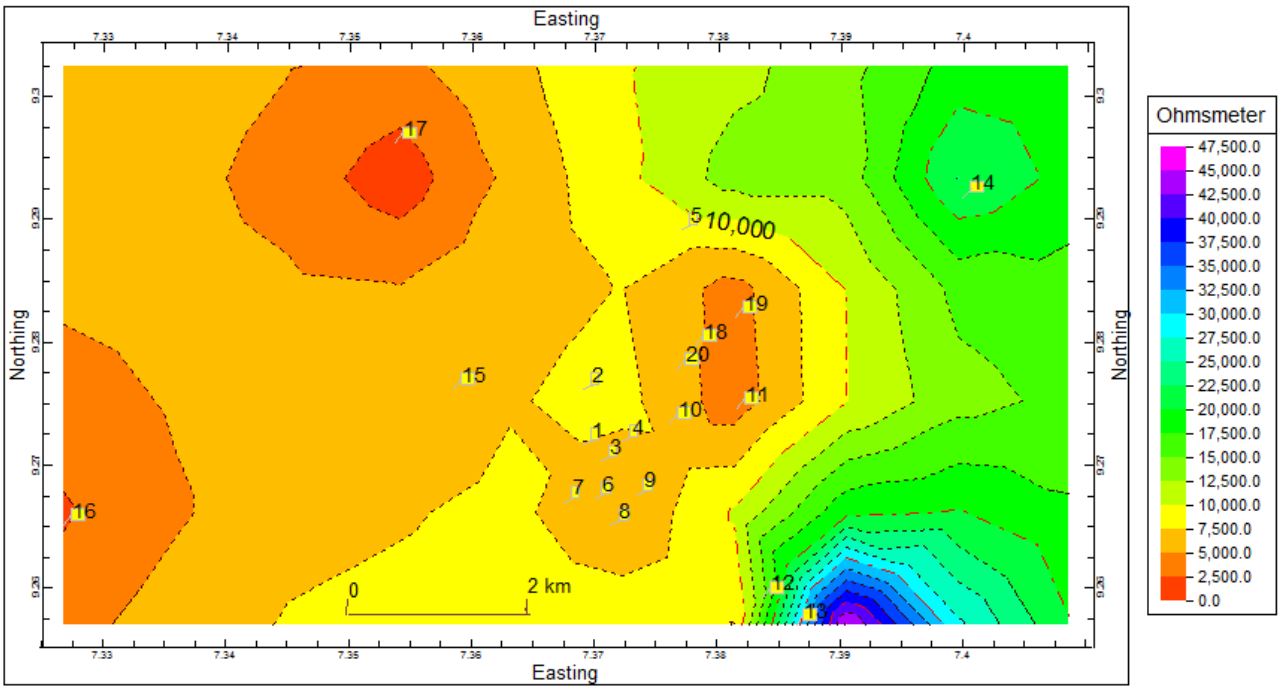

Figure 12. Spatial distribution of transverse resistance of the study area.

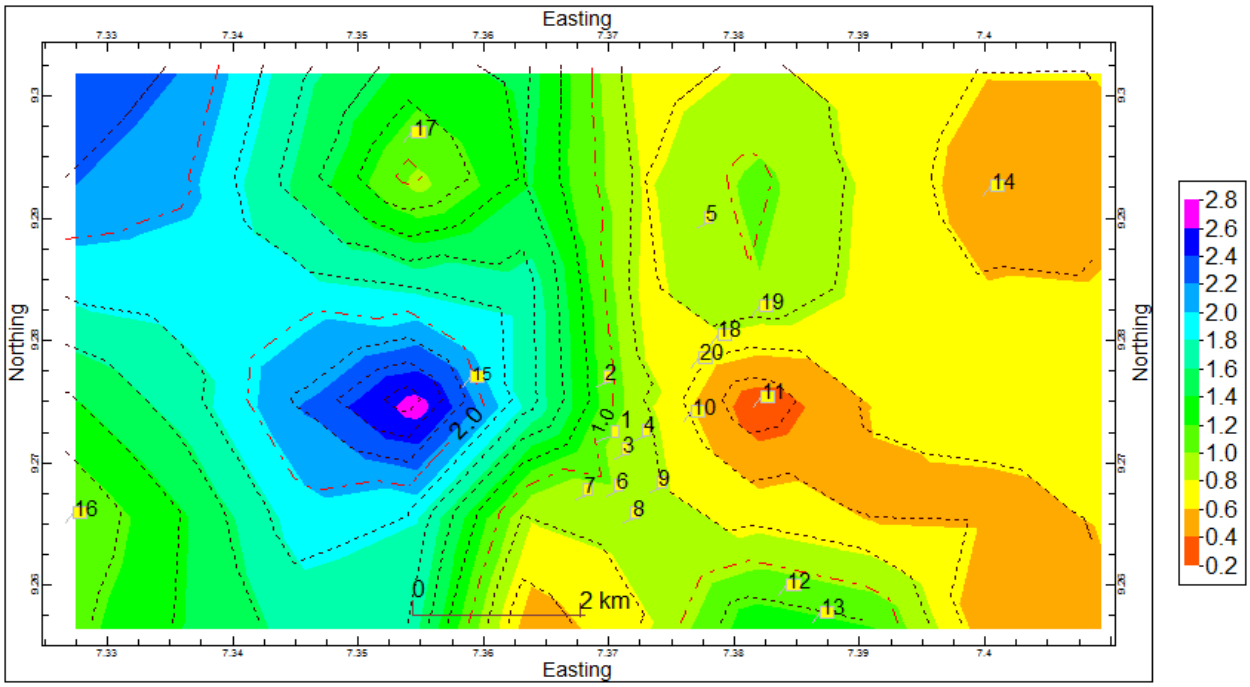

Figure 13. Spatial distribution of coefficient of anisotropy of the study area.

Conclusions

Groundwater usually occurs in discontinuous aquifers in basement complex area. Defining the potentials of the aquifers is normally a tedious exercise because of the intricate properties of the basement rocks. The integration of various electrical resistivity parameters have shown to be efficient in classifying the groundwater

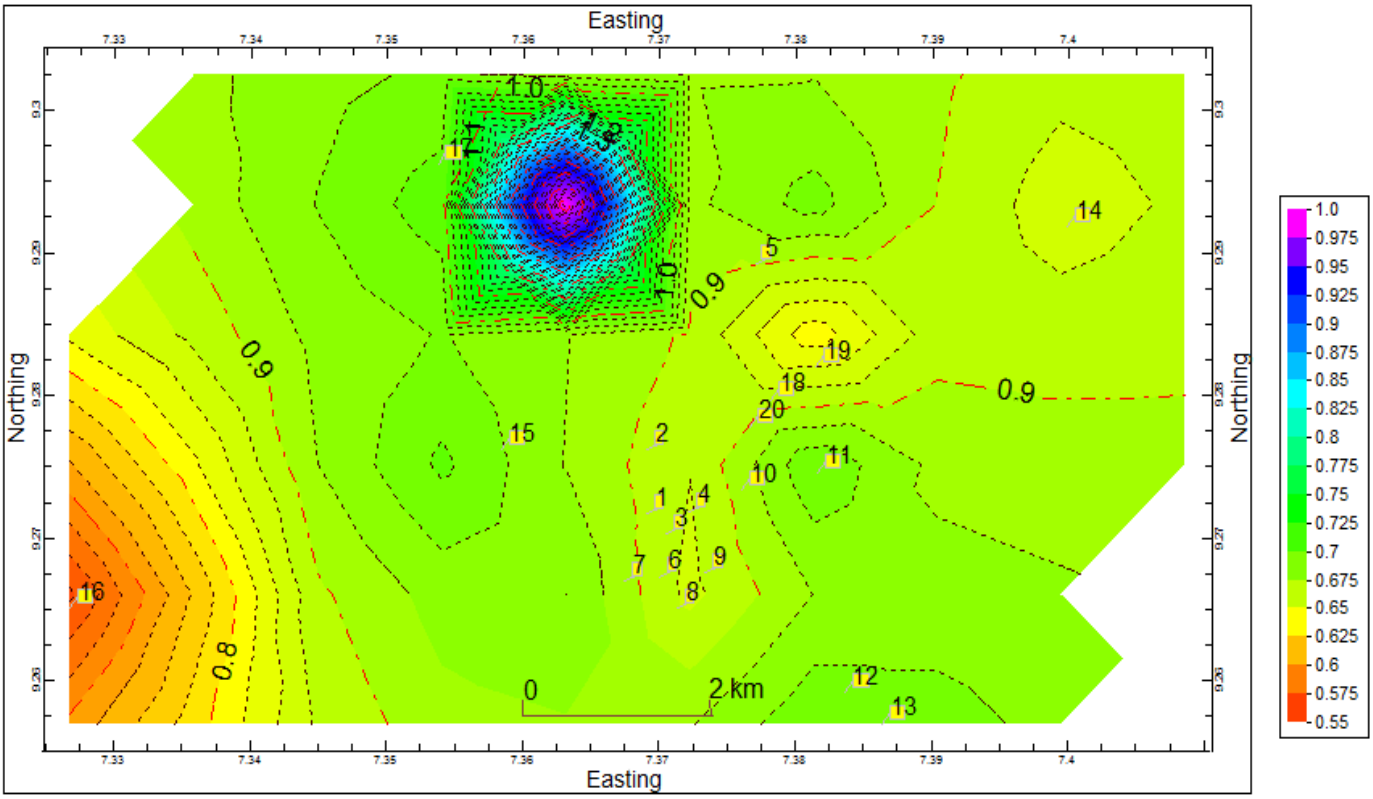

Figure 14. Spatial distribution of reflection coefficient of the study area.

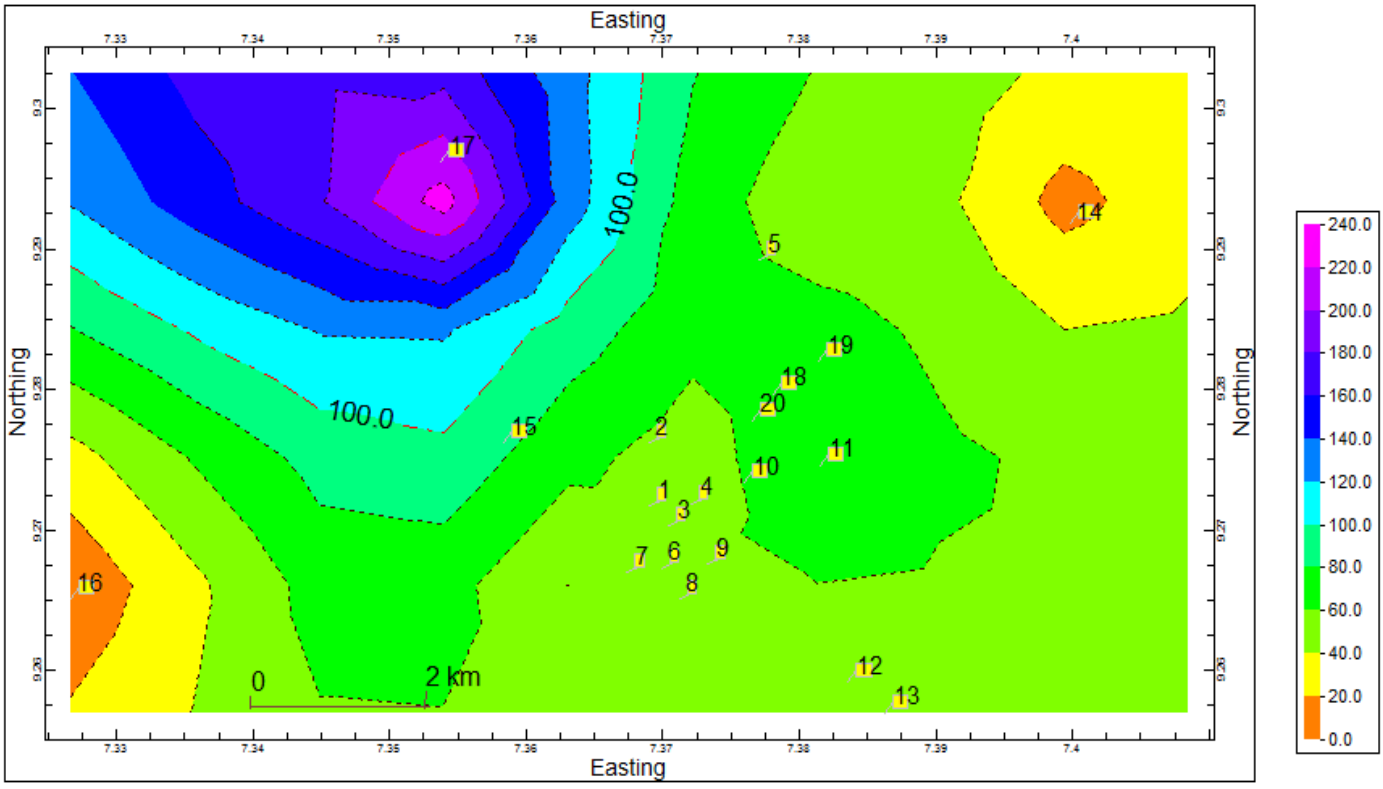

Figure 15. Spatial distribution of resistivity contrast of the study area.

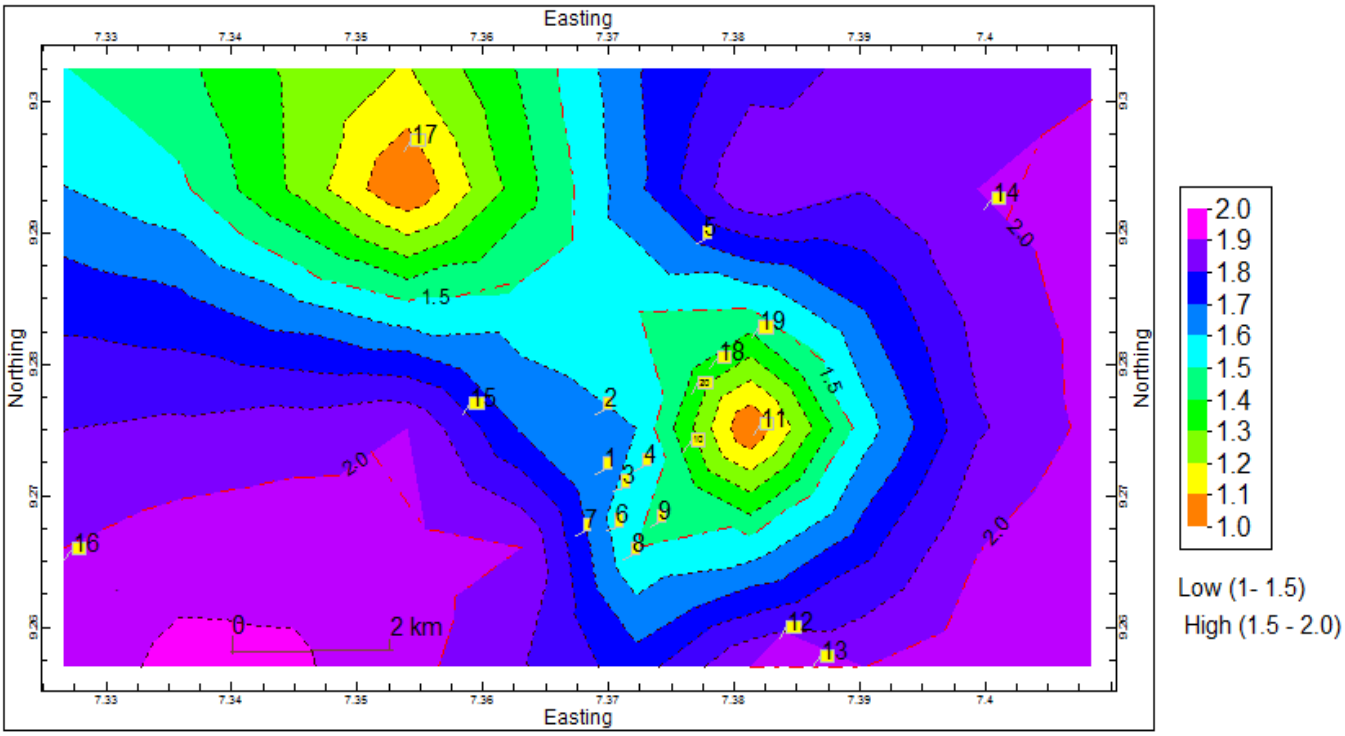

Figure 16. Groundwater potentials of the study area.

potentials of a basement terrain. Groundwater developments should be concentrated in areas of high groundwater potentials and conjunctive use of surface water should be encouraged to reduce complete dependence on groundwater.

REFERENCES

Anudu GK, Onuba LN, Ufondu LS (2011). Geoelectric Sounding for Groundwater Exploration in the Crystalline Basement Terrain Around Onipe and Adjoining Areas, Southwestern Nigeria. J. Appl. Technol. Environ. Sanitation 1(4):343-354.

Bhattacharya PK, Patra HP (1968). Direct Current Geoelectric Sounding Methods in Geophysics. Elsevier, Amsterdam P.125.

Keller GV, Frischknecht FC (1966). Electrical methods in geophysical prospecting, Pergamon press, New York pp. 179-187.

Kumar MS, Gnanasundar D, Elango L (2001). Geophysical studies to determine hydraulic characteristics of an alluvial aquifer. J. environ. hydrol. 9(15):1-7.

Loke MH (1999). Electrical Imaging surveys for environmental and engineering studies. A practical guide to 2-D and 3-D surveys: Pre-conference workshop notes W2, The theory and practice of electrical imaging, EEGS-European Section 5th Meeting, Budapest, Hungary.

Mabogunje AL (1977). Report of the ecological survey of the Federal Capital Territory, Abuja, 1: The Environment; Planning Studies Programme, University of Ibadan.

MDG (2012). www.mdgfctabuja.net viewed on the 23rd September, 2012.

Okhue ET, Olorunfemi MO (1991). Electrical resistivity investigation of a typical basement complex area- The Obafemi Awolowo University campus case study. J. Mining Geol. 27(2):66-70.

Olayinka AI (1996). Non Uniqueness in the Interpretation of Bedrock Resistivity from Sounding Curves and its Hydrological Implications. Water Resour. J. NAH. 7(1-2):55-60.

Olayinka AI, Obere FO, David LM (2000). Estimation of longitudinal resistivity from Schlumberger sounding curves. J. Mining Geol. 28:403-412.

Rahaman MA (1989). Review of the Basement Geology of southwestern Nigeria. In: Kogbe, C. A. (ed.). Geology of Nigeria, 2nd revised edn. Rockview Nigeria Limited, Jos: 39-54.

Rao JP, Rao SB, Rao JM, Harikrishna P (2003) .Geo-electrical data analysis to demarcate groundwater pockets and recharge zones in Champavathi River Basin, Vizianagaram District, Andhra Pradesh. J. Indian Geophys. Union 7(2):105-113.

Todd KD, Mays LW (2005). Groundwater Hydrology. 3rd ed. John Wiley and Sons, New York. P. 636.

Todd KD (1980). Groundwater Hydrology. 2nd ed. John Wiley and Sons, New York P. 535.

Zohdy AAR, Martin RJ (1993). A study of sea water intrusion using direct current sounding in the Southern part of the Ox ward Plain California. Open-file reports 93 – 524 U. S. Geological Survey P. 139.

Zohdy AAR, Eaton GP, Mabey DR (1974). Application of surface geophysics to groundwater investigations: Techniques of water resources investigations of the United Geophysical Survey Book. United States Government Printing Office, Washington DI, P. 116.

academicJournals

Vol. 8(25), pp. 1362-1370, 9 July, 2013
DOI: 10.5897/IJPS2013.3942
ISSN 1992 - 1950 © 2013 Academic Journals
http://www.academicjournals.org/IJPS

International Journal of Physical Sciences

Full Length Research Paper

Experimental study of air-water turbulent flow structures on stepped spillways

Mohammad Reza Beheshti[1]*, Amir Khosrojerdi[1] and Seyed Mahmud Borghei[2]

[1]Department of Water Science and Engineering, Science and Research Branch, Islamic Azad University, Tehran, Iran.
[2]Department of Civil Engineering, Sharif University of Technology, Tehran, Iran.

Accepted 17 June, 2013

Stepped chute flows are characterized by intense turbulence and strong flow aeration, but most studies did not investigate the turbulence characteristics. In this study, highly turbulent air-water flows skimming down a large-size stepped chute were systematically investigated. An experimental study of detailed air-water flow properties measurements were introduced in different types of flow regimes on a stepped chute (θ = 21.8°, h = 0.04 m, l = 0.10 m) model to investigate the location and the flow depth at inception point of air entrainment and velocity profiles distributions. Detailed velocity and turbulence intensity measurements in flow direction were performed by use of a phase detection conductivity probe which was designed, developed and calibrated by writers. The results showed that the turbulence characteristics vary in different regions. The study showed further that the turbulence intensity increases rapidly close to the step bottom at the viscous sub layer and maximized for 0.4 ≤ y/dc ≤ 0.5 at intermediate region then decreases gradually in the upper region. It is hypothesized that the high turbulence levels in the intermediate region were caused by the continuous deformations and modification of the air-water interfacial structure.

Key words: Air-water flows, conductivity probe, inception point, stepped chute, turbulence intensity.

INTRODUCTION

The interactions between flowing waters and atmosphere may lead to strong air-water mixing and complex multiphase flow situations. The evaluation of the air-water flow properties is particularly important on stepped spillways over RCC dams experiencing moderate unit discharges, because large quantities of air entrain upstream of the spillway toe.

Numerous studies of stepped spillway flows were conducted with different approaches over the past forty years. Studies of spillways with particular focus on stepped chutes include Sorensen (1985), Peyras et al. (1991), Christodoulou (1993), Chamani and Rajaratnam (1999), Chinnarasri and Wongwises (2006), Relvas and Pinheiro (2011), and others. Only a limited number of published papers refer to highly turbulent flows associated with strong free-surface aeration (Chanson and Toombes, 2002; Yasuda and Chanson, 2003).

In civil engineering applications, the flow velocity exceeds typically 5 to 10 m/s, the flow Reynolds number ranges from 1 E+7 to over 1 E+9 in large dam spillways, and free-surface aeration is nearly always observed. Such high-velocity highly-aerated flows cannot be studied analytically or numerically because of the large number of relevant equations and parameters. Current knowledge

*Corresponding author. E-mail: mr.beheshti@ sr.iau.ac.ir.

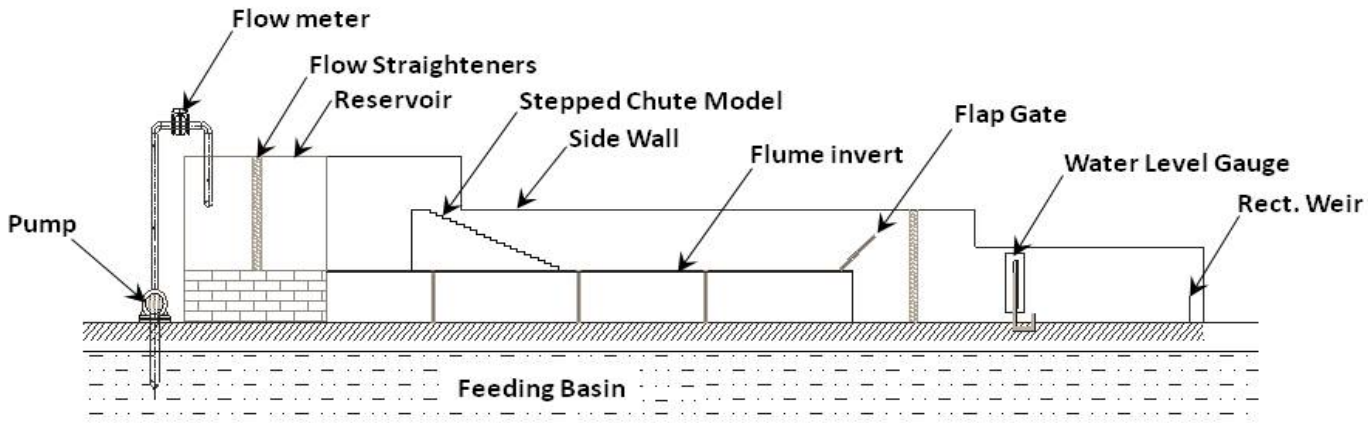

Figure 1. The experimental set-up of the stepped spillway (Hydraulic laboratory of WRI, Tehran, Iran).

relies upon physical modeling and experimental measurements. Accurate measurement systems for air-water flow measurements are limited to intrusive phase-detection probes, hot-film probes, and LDA/PDA systems.

According to the literature review, the measurement of the flow velocity concerns only the longitudinal component, parallel to the mean slope. Double fiber-optical and double-tip conductivity probe are at the moment the more efficient intrusive instrumentation to measure the mixture flow velocity. In fact, the Prandtl tube or back-flushing Pitot tube is limited to low aerated flow (that is, for air concentration less than 0.7).

In the present study, new experiments were conducted in a large stepped channel with a 21.8° slope and it is shown that the advanced developed dual-tip conductivity probe may provide new information on the air-water turbulent characteristics on stepped chutes. Detailed air-water flow properties were recorded systematically for several flow rates including turbulence levels, void fractions and velocity distributions. The results provide a new understanding of the complicated air-water structure on stepped spillways.

MATERIALS AND METHODS

Experimental setup

The experiments were conducted in a rectangular Perspex-walled flume in the Hydraulics laboratory at the water research Institute of Iran Power Ministry. The experimental channel was 5 m long and 0.90 m wide. Water flow was supplied from a large feeding basin under the laboratory leading to a concrete reservoir upstream of the flume.

The test section consisted of a broad crested weir (0.83 m wide, 0.45 m long, with upstream sharped corner) followed by twenty identical steps (h = 0.04 m, l = 0.10 m) made of Plexi-Glass plates. The stepped chute was 0.83 m wide with Perspex sidewalls followed by a horizontal steel-invert flume ending in a dissipation pit (Figure 1). The physical model is part of a closed water cycle.
The chute bottom angle, equal to the pseudo-bottom angle, was φ = 21.8° (1V : 2.5H).

The measurement reach located at 3.5 from the entrance channel section, was 3 m long. A pump controlled with an adjustable frequency AC motor drive delivered the flow rate, enabling an accurate discharge adjustment in a closed-circuit system.

At the downstream end of the flume, the tail gate controls the tail water depth. For all measurements, the gate was fully opened.

Instrumentation and measurement techniques

In present study, the measured parameters are included: clear-water flow depths, clear-water and air-water flow velocities and flow rate.

Clear-water flow depths were measured using a rail mounted vertical pointer gauge with 1 mm accuracy. Clear-water velocities were measured with a Pitot tube (3.3 mm external diameter, 20 mm distance between tip and lateral holes). The flow rate measurements were performed using a rectangular sharp-crested weir located in the outlet channel and an electromagnetic flow meter positioned in the inlet pipe, used for confirmation of the weir discharge measurements. Detailed information about air-water flow properties like the air-water flow velocity, the air concentration and bubble sizes and frequencies was gained using a double-tip conductivity probe (Ø = 0. 7 mm) which was developed and calibrated at Science and Research Branch of Islamic Azad University by authors.

The conductivity probe is a phase-detection intrusive probe designed to pierce the bubbles. The phase-detection relies on the difference in electrical resistance between air and water. The probe mounted on a support frame parallel to the chute slope and consists of two identical tips made of stainless steel surgical needle. The tips are aligned in the flow direction and the distance between the tips is 4 mm (Figure 2). The sampling frequency of the developed probe is 50 kHz with adjustable sampling time. The two-phase flow properties measurements were taken from the tip of the steps to as close to the water surface as possible. All measurements were performed on the channel centerline (z = 0) at step edges and adjacent step edges.

Experimental flow conditions

In the stepped chute, the basic flow regimes were inspected in a series of visual observation with discharges ranging from 0.012 m^3/s to 0.035 m^3/s (Table 1). The model development was based on the Froude similitude. The facility was designed to operate with flow conditions ranging from nappe to skimming flow regimes. The

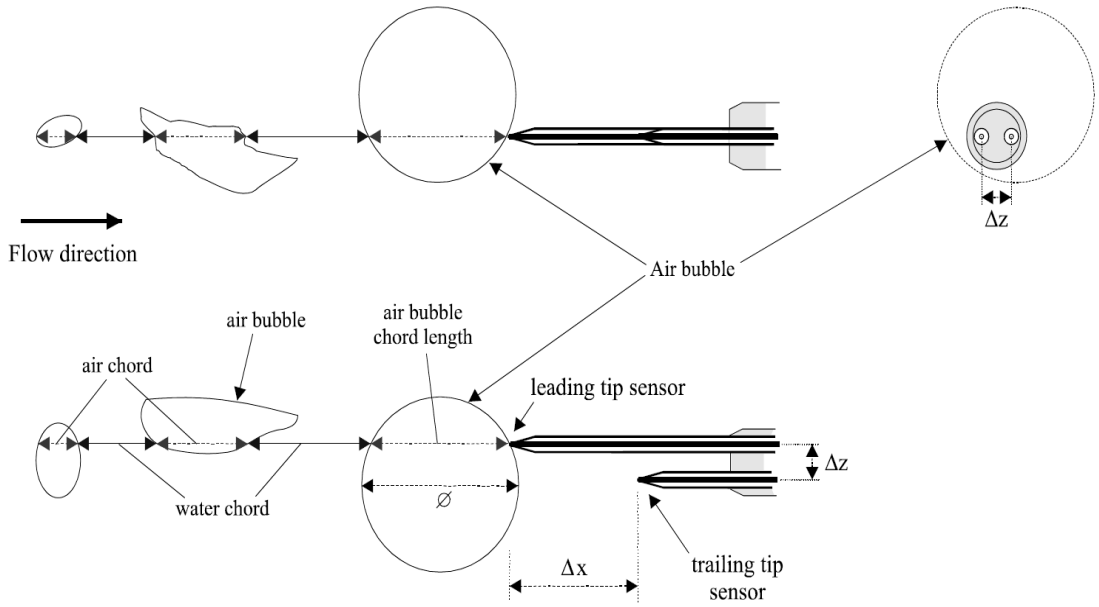

Figure 2. Sketch of the double-tip conductivity probe and its operation.

Table 1. Summary of experimental flow conditions (Present study).

Q_w, m³/s (1)	q_w m³/s/m (2)	d_c/h (3)	Re (4)	We (5)	Flow regime (6)	Location of inception of air entrainment (7)	Remarks (8)
0.012	0.0147	0.701	5.8×10^4	102.519	Nappe Flow	Step edge 4	W = 0.83 m, h = 0.04 m, l = 0.10m
0.015	0.0184	0.813	7.2×10^4	109.975	Transition Flow	Step edge 4	W = 0.83 m, h= 0.04 m, l = 0.10m
0.020	0.0241	0.981	9.6×10^4	119.380	Transition Flow	Step edge 6	W = 0.83 m, h= 0.04 m, l = 0.10m
0.025	0.0301	1.131	1.2×10^5	119.788	Skimming Flow	Step edge 7	W = 0.83 m, h= 0.04 m, l = 0.10m
0.030	0.0361	1.282	1.4×10^5	204.789	Skimming Flow	Step edge 7	W = 0.83 m, h= 0.04 m, l = 0.10m
0.035	0.0422	1.415	1.7×10^5	314.580	Skimming Flow	Step edge 8	W = 0.83 m, h= 0.04 m, l = 0.10m

flow conditions corresponded to flow Reynolds numbers ranging from 5.8×10^4 to 1.7×10^5. The Reynolds number defined in terms of the hydraulic diameter as:

$$R_e = V \times D_H / u_w \quad (1)$$

Where D_H is the hydraulic diameter, V and u_w are the interfacial velocity and the kinematic viscosity of the water, respectively.
The measured flow rates, and other experimental parameters of the different conditions, are shown in Table 1.

Data processing

Air-water flow properties were recorded for nappe (that is, dc/h < 0.701), transition (0.701 < dc/h < 0.1.131) and skimming flows (that is, dc/h > 1.131). In rectangular channels, the critical depth is estimated by $d_c = \sqrt[3]{q_w^2 / g}$ where q_w is the water discharge per unit width and g is the gravity acceleration.

During each test, photographic observations recorded the inception point of air entrainment. The inception point was noted as the location where the flow changed from a glassy, smooth appearance to a more frothy appearance at the free surface. The inception point location was described quantitatively by its horizontal distance from the spillway crest and with regards to step location within the spillway chute. On stepped spillways, the position of the start of air entrainment is a function of the discharge, spillway roughness, and step geometry.

Velocity measurement is based upon the successive detection of air-water interfaces by two tips. This technique assumes that the probe tips are aligned along a streamline and that bubbles and droplets are little affected by the leading tip. When a proportion of bubbles strike the leading tip and trailing tip sequentially, the resulting signals from the two tips will be similar with a slight time delay. This time delay is the average time for a bubble to travel the distance between the two tips. If this distance is known, the time can be converted into a mean air-water interface velocity.
The time-averaged air-water velocity equals:

$$V = \frac{\Delta X}{T} \quad (2)$$

Where Δx is the longitudinal distance between probe sensors (Figure 2) and T is the air-water travel time between the two probe sensors. Air-water flow characteristics data were collected at 50 KHz frequency with a sampling duration of 90 s. The data analyses were done in Excel spread sheets and Grapher V.9.1.536 software.

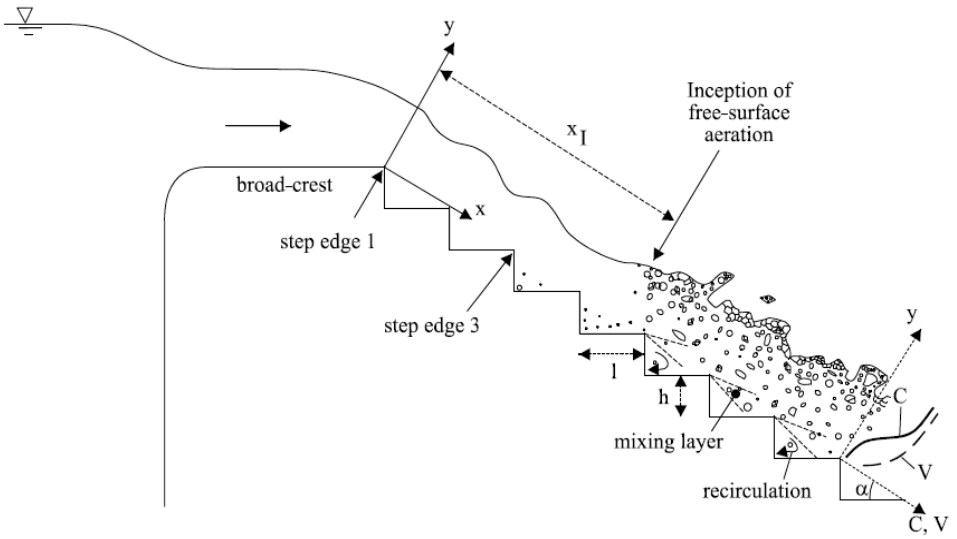

Figure 3. Definition sketch of flow over stepped chute.

In analysis, the distribution of the time averaged velocity, air concentration, fluctuating velocities and turbulence intensities as well as their decay along the downstream direction were considered.

EXPERIMENTAL RESULTS AND DISCUSSION

Detailed measurements of air-water flow properties were conducted for a number of dimensionless flow rates (d_c/h).

The maximum water heads above the spillway crest are between 86.25 and 93.95 cm (measured from the toe of the spillway as the datum) and corresponding unit width discharges between 0.0147 and 0.042 $m^3/s/m$. The approach flow conditions corresponding to Froude numbers between 0.643 and 1.007.

A right hand coordinate system was adopted at measuring sections in the flume with x-axis as the streamwise distance along the channel bottom, y-axis as the distance measured normal to the invert (or channel bed) and z-axis as the transverse distance from the channel centerline.

The dimensionless distributions of interfacial velocity and turbulent intensity showed some characteristic features.

Basic flow observations

Flow regimes

For a given chute geometry, the flow pattern above a stepped channel may be nappe flow, transition flow or skimming flow. The type of flow regime is a function of the discharge and step geometry (Chanson, 1994b; Chanson and Cummings, 1996). For low discharges, the water flow drops from step to step on a stepped chute. That is the nappe flow regime which was studied by Chamani and Rajaratnam (1994), Chanson (1994a), Toombes (2002), El-kamash et al. (2005), and Toombes and Chanson (2008).

For some intermediate discharge, the transition flow regime is observed which is characterized by a chaotic behavior and strong splashing and droplet projections downstream of the inception point of free surface aeration (Chanson, 2001b, Chanson and Toombes 2004). For this regime, the flow can appear as nappe flow (presence of air caity) for some steps and as skimming (onset of vortices in a filled step) for the rest. For larger flows, the waters skim above the pseudo-bottom formed by the step edges.

The skimming flow is characterized by strong cavity recirculation with three-dimensional vortical patterns (Rajaratnam, 1990; Chanson 1994b, 1995a; Chamani and Rajaratnam, 1999). The flow regime changes in the stepped chute was observed and analyzed in this study. The conditions linked to the flow configuration changes have been quantitatively studied. The parameters which have been considered to quantify these changes are the ones related to flow critical depth (dc) and to the spillway geometry, which are the non-dimensional ratios d_c/h and h/l where dc is the critical depth and h and l are the step height and length respectively. A sketch of stepped chute flow and other geometrical parameters are shown in Figure 3.

A nappe flow regime without hydraulic jump was observed for small flow rates ($d_c/h < 0.813$) and for large flow rates ($d_c/h > 1.131$), the water skims over the pseudo-bottom. At moderate discharge rates ($0.813 < d_c/h < 1.131$), a transition flow pattern was observed. The non-dimensional characteristic depth (d_c/h) values corresponding to the different flow regime observations

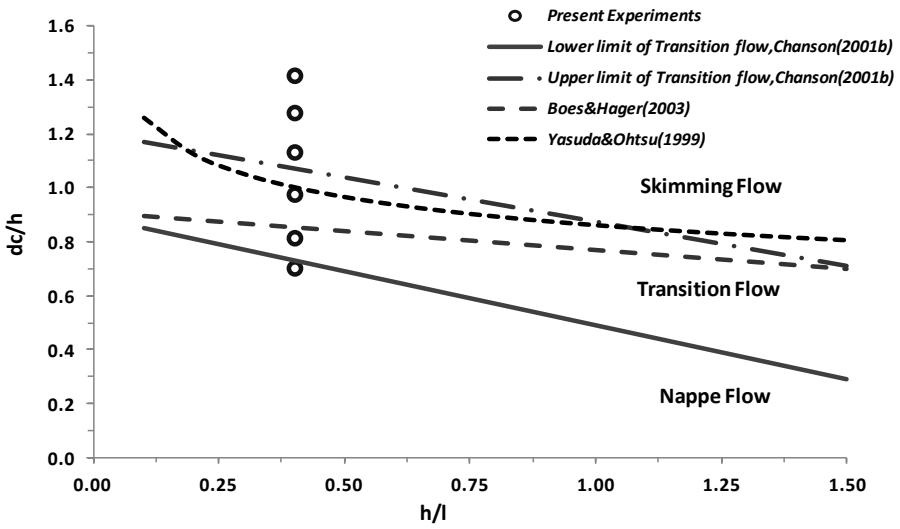

Figure 4. Flow regimes estimation on the stepped chute and comparison with the empirical relationships.

are shown in Figure 4 and compared with some researchers' observations.

The observation results for flow regime prediction were in agreement with onset/transition functions in the literature (Chanson, 1995a, 2001b).

Characterizing the inception point of air entrainment

At the upstream end of the stepped spillway, a turbulent boundary layer is generated by bottom friction and it develops in the flow direction. When the outer edge of the developing boundary layer reaches the vicinity of the free-surface, air entrainment is initiated.

This location is called the inception point of free-surface aeration. Downstream, the turbulence next to the free-surface is large enough to initiate substantial flow aeration. In the present study, the location of the inception point of free-surface aeration was recorded in all flow regimes. At the inception point, the air is entrained into the flow owing to a large degree of turbulence.

Determination of the inception point location along the spillway is important to estimate the unaerated zone, which is prone to the cavitation damage. Cavitation is a serious problem resulting from hydrodynamic pressures, on the step surfaces or at the step edges, which could fall below the vapor pressure (Boes and Hager, 2003).

Cavitation might cause severe damage to the steps and can be mitigated by a significant aeration along the spillway. Prevention of cavitation potential damage requires a mean air concentration of at least 5 to 8% (Peterka, 1953). For all the current models experiments, the location of the inception point was defined by visual observation and pointer gauge measurements of the water surface where the air was entrained into the flow for the whole spillway width. The non-dimensional parameter x_I/k_s, is plotted as a function of the roughness Froude number (Fr*) in Fig. 5 for current experimental data. The parameter k_s is defined as the step roughness height and equals to hcosθ. Fr* is a Froude number defined in terms of the step roughness:

$$F_r* = q_w \Big/ \sqrt{(h\cos\theta)^3 g \sin\theta} \quad (3)$$

The available literature data are also shown in Figure 5 and compared with the current data. Figure 5 shows there are good agreement of the results with Boes and Hager (2003) and a fair agreement with others. For the present study, the results were best correlated by the following equation to locate the inception point of air entrainment on the 21.8° stepped chute for 0.701<dc/h<1.415:

$$\frac{X_I}{K} = 8.0833 \mathrm{E}_*^{0.7723} \quad (4)$$

Interfacial velocity and turbulent intensity distributions

In analogy with the studies of uniform rough flow for steep gravel beds in mountain streams, a few authors (Chamani and Rajaratnam, 1999) suggested that above the pseudo-bottom, the homogeneous air-water flow agrees with the rough boundary layer theory. However, because of the high relative roughness of the steps, the 3D pattern of the macro-turbulence structures as well as

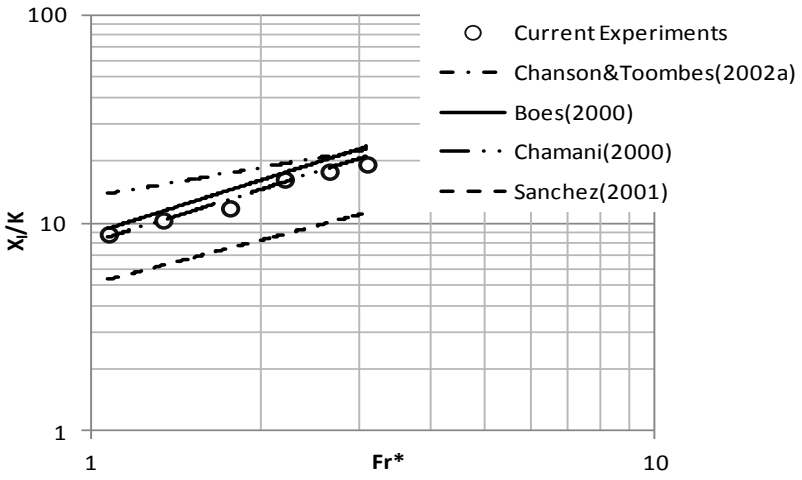

Figure 5. Dimensionless location of the inception point of free-surface aeration.

Table 2. Comparison of the power law coefficients for velocity distribution.

References	D	N	Remarks
Chanson (2001b)	1	5~6	Skimming flow
Chamani and Rajaratnam(1999)	1	6.3	$\theta = 30°$
Boes(2000)	1	6.3	$0.04 \le Y_{90} \le 0.5$
Boes and Hager (2003)	1.05	4.3	$0.04 \le Y_{90} \le 0.8$, $26° \le \theta \le 55°$
Yasuda and Chanson (2003)	1	9	$0.05 \le Y_{90} \le 1$, $\theta = 15.6°$
Current Study	1.012	5.21	$0.03 \le Y_{90} \le 0.92$, $\theta = 21.8°$

the drag around steps, the classical logarithmic equation as proposed by Karman-Prandtl is not fully applicable.

$$\frac{v(x)}{\sqrt{\tau_o / \rho_w}} = \frac{2.30}{\kappa} \log\left(\frac{x}{\kappa}\right) + C1 \quad (5)$$

In which k is the von Karman turbulence constant determined experimentally between 0.40 and 0.42,
C1 an integration constant, k the equivalent roughness size and τ_0 the boundary shear stress.

Nevertheless, most researchers proposed that above the pseudo-bottom the local mixture velocity depends on the maximum velocity and that the velocity distribution follows a power law given by:

$$U_{90} = DY_{90}^{1/N} \quad (6)$$

Where $U_{90} = \frac{u}{u_{90}}$ and $Y_{90} = \frac{y}{y_{90}}$ are the dimensionless mixture flow velocity and depth respectively. u_{90} and y_{90} are the velocity and flow depth corresponding to 90% air concentration. D and N are coefficients obtained from experiments data. This result has been validated for model and prototype data of air-water open channel flows by several other researchers, including Chanson (1989), Wood (1991) and Chanson and Cummings (1996). However, depending on the tested discharges or the portion of flow layer considered in the empirical fitting, several power laws have been proposed with different coefficients and some of them were listed in Table 2.

In the present study, the velocity power law exponent was 1/5.21 in average (that is, N = 5.21), although it varied between adjacent step edges. Such fluctuations were believed to be caused by some interference between adjacent shear layers and cavity flows. In current study, the velocity distributions at each step edge compared favorably with the power-law function for $y/y_{90} < 1$ and with a uniform profile for $y/y_{90} > 1$:

$$\left(\frac{u}{u_{90}}\right) = D\left(\frac{y}{y_{90}}\right)^{1/N}, \quad 0 \le \frac{y}{y_{90}} \le 1 \quad (7)$$

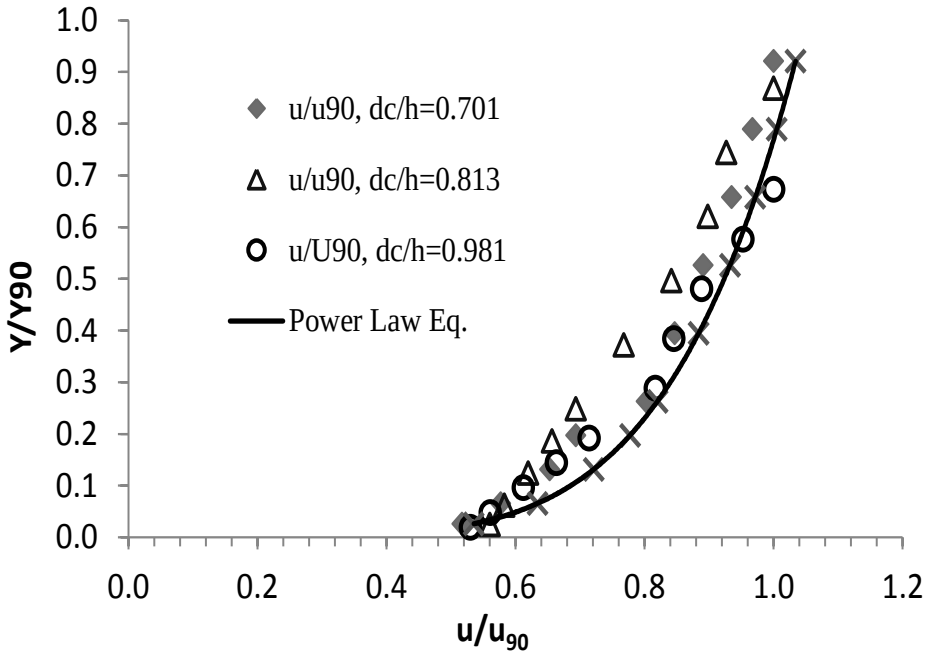

Figure 6. Dimensionless distributions of normalized interfacial velocity u/umax in different flow regimes at step edge 15.

$$\left(\frac{u}{u_{90}}\right)=1 \ , \quad 1\le\frac{y}{y_{90}}\le 2.5 \tag{8}$$

Equation (7) is compared with experimental data in Figure 6 for several dimensionless discharges dc/h. The data does not include the profiles closest to the sidewall, which are likely affected by sidewall friction. In nappe and transition flows, the velocity measurements show quasi-uniform velocity profiles at step edges (Figure 6).

The result is relatively close to that of Chanson and Toombes (2002). It has no theoretical justification and it is only a rough correlation. The velocity distribution results in skimming flows are basically identical to measured velocity distributions in self-aerated flows on smooth-invert chutes (Cain, 1978), although the rate of energy dissipation is much greater on a stepped cascade and flow resistance is dominated by form drag.

Due to turbulent eddies; the local instantaneous flow velocity (u) within the boundary layer will fluctuate in a more or less random fashion. However, the velocity record for turbulent flow includes both a mean and a turbulent component.

The decomposition of the flow velocity is as follow:

$$u=\bar{u}+u' \quad \rightarrow \quad u'=u-\bar{u} \tag{9}$$

This is commonly called a Reynolds' decomposition, where:

$\bar{u}=$ Time-averaged velocity which equals to $\lim_{T\to\infty}\frac{1}{T}\int_0^T u(t)dt$

$u'=$ Velocity fluctuation in the stream-wise direction also called as characteristic turbulent velocity.

T= sampling time

Two methods are used to describe the turbulence of the flow; single point observations and correlations between multiple points. The more common method uses measurements of velocity fluctuations at one point in the flow. So, an accurate measure of the turbulent intensity can be obtained.

Herein, the turbulent intensity is defined in terms of the statistical quantities which describe the random fluctuations. A convenient measure of the fluctuating component of the flow velocity is the root-mean-square value as below:

$$u'_{rms}=\sqrt{\overline{u'^2}}=\sqrt{\frac{\sum_{i=1}^{n}\left(u_i-\bar{u}\right)^2}{n}} \tag{10}$$

Where n is the number of samples.

The normalized turbulence intensity in flows over a spillway dam is subject to the influence of flow patterns of the boundary layers as well as boundary conditions of different sections (e.g. the dam crest, downstream slope, surface roughness). Turbulence Intensity is a dimensionless measure of the turbulent fluctuations of

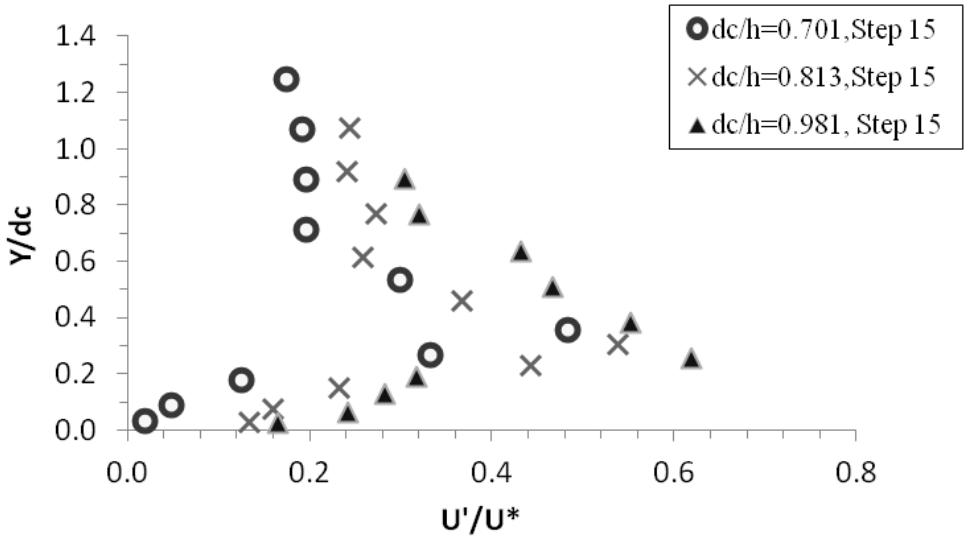

Figure 7. Vertical distribution of turbulence intensity in air-water flow over steps.

interfacial velocity which characterizing turbulence and defined as the root-mean-square value of the fluctuations in the flow direction divided by the shear velocity.

$$T_U = \frac{u'_{rms}}{u*} \quad (11)$$

Where the u* is the shear or friction velocity and can be determined from the boundary shear stress distribution based upon the friction slope S_f, if the flow is gradually varied.

The shear velocity have a great impact on the distribution of the mean velocity and turbulence structure in the boundary layer and is the most fundamental velocity scale with which to normalize mean velocity and turbulence.

$$u* = \sqrt{\tau_o / \rho_w} \quad (12)$$

$$\tau_0 = g\rho_w S_f \int_{y=0}^{y=y_{90}} (1-C)dy \quad (13)$$

Where the frictions slope $S_f = -\frac{\partial H}{\partial x}$ is the slope of the total head line.

Figure 7 shows the normalized turbulent intensities (Tu) distributions at different verticals and relative discharges (d_c/h). The data were obtained at step edges and at the same dimensionless distance from the inception point.

It can be seen from Figure 6 that the turbulence characteristics vary in different regions. Herein, the turbulence intensity increases rapidly close to the step bottom at the viscous sub layer and maximized for 0.4≤ y/dc ≤ 0.5 at intermediate region then decreases gradually in the upper region. A similar trend was observed in previous studies (Chanson and Toombes, 2002; Gonzalez, 2005; Chanson and Carosi, 2007a). It is hypothesized that the high turbulence levels in this intermediate region were caused by the continuous deformations and modification of the air-water interfacial structure.

Conclusions

Flows cascading down a stepped spillway with a moderate slope are characterized by some strong aeration and high turbulence of the flow. In this study, a set of air-water flow experiments were preformed in high velocity flows on a relatively large stepped channel based on Froude similitude.

The two phase flow measurements were preformed with a conductivity double-tip probe downstream of the inception point of aeration. The results included air water flow properties such as air concentration, flow velocity, turbulence, and bubble count rate. Based on measured air-water velocities, the flow shear stress, friction velocity and turbulence intensities were estimated accurately. The air-water flow properties presented some basic characteristics that were qualitatively and quantitatively in agreement with previous studies. High turbulence levels were recorded downstream of the aeration inception point. The distributions of turbulence intensity had a similar shape as clear-water flow data of Ohtsu and Yasuda down a stepped chute.

The measurements showed that immediately downstream of the inception point of air entrainment, the flow is rapidly varied and the maximum turbulence intensities occurred in the intermediate region between the spray and bubbly flow regions (that is, 0.3 < C < 0.7).

Although the findings were obtained for a moderate slopes (θ = 21.8°), it is believed that the outcomes are valid for a wider range of chute geometry and flow conditions typical of embankment chutes.

ACKNOWLEDGEMENT

The funding for these and related studies was provided by the Guilan Regional Water Company. Also, the authors acknowledge the helpful discussion with Prof. Chanson and Mr. Reza Rushan (Head of Hydraulics structures Department of the Water Research Institute, Power Ministry, Tehran, Iran).

Nomenclature: C, Void fraction defined as the volume of air per unit volume; **DH,** hydraulic diameter (m); **d,** characteristic depth (m); **dc**, critical flow depth (m); **Fr*,** Froude number defined in terms of the roughness height; **H,** total head (m); **Hmax,** maximum head available (m) using the spillway toe as datum; **H,** height of steps (m) (measured vertically); **ks,** step dimension (m) measured normal to the flow direction; **l,** length of steps (m) (measured horizontally); **Qw,** water discharge (m^3/s); **qw,** water discharge per unit width (m^2/s); **Re,** Reynolds number defined in terms of the depth-averaged flow velocity and **Sf,** hydraulic diameter friction slope; **T,** sampling time(s); **Tu,** turbulence intensity; **Uw,** equivalent clear-water flow velocity (m/s); **u',** root mean square of longitudinal component of turbulent velocity (m/s); $\bar{u}$, time-averaged velocity(m/s); **u*,** shear or friction velocity(m/s); **W,** stepped spillway width (m); **we,** Weber number; **x,** longitudinal/streamwise distance (m); **xI,** distance (m) from the start of growth of boundary layer to the inception point of air entrainment; **y,** distance (m) from the pseudo-bottom (formed by the step edges) measured perpendicular to the flow direction; y_{90}, characteristic depth (m) where the air concentration is 90%; τ_0, boundary shear stress (Pa).

Subscripts: c, Critical flow conditions; **f,** friction; **I,** characteristics of the inception point; **l,** a discrete point; **max,** maximum value in a cross-section; **rms,** root mean square; **w,** water flow; **90,** flow conditions where C = 0.90.

REFERENCES

Boes M (2000). Role of natural and immune IgM antibodies in immune responses. Mol. Immunol. 37:1141–1149.

Boes RM, Hager WH (2003). Hydraulic Design of Stepped Spillways. J. Hydr. Eng. pp. 671-679.

Chamani MR, Rajaratnam N (1994). Jet Flow on Stepped Spillways. J. Hydr. Eng. A.S.C.E. 120(2):254-259.

Chamani MR, Rajaratnam N (1999). Characteristics of Skimming Flow over Stepped Spillways., J. Hydr. Eng. ASCE. 125(4):361-368.

Chanson H (1989). Study of Air Entrainment and Aeration Devices. J. Hydr. Res. IAHR. 27(3):301-319.

Chanson H (1994a) "Hydraulic Design of Stepped Cascades, Channels, Weirs and Spillways, Pergamon, Oxford, UK, Jan. P.292 (ISBN 0-08-041918-6).

Chanson H (1994b). Hydraulics of Skimming Flows over Stepped Channels and Spillways, J. Hydr. Res. 32:445-460

Chanson H (1995a). Hydraulic Design of Stepped Cascades, Channels, weirs and Spillways, Pergamon, Oxford, UK.

Chanson H (2001b). A Transition Flow Regime on Stepped Spillways? The Facts. In Proceedings of the 29th IAHR Biennial Congress, Beijing, China, Theme D. Vol.1. Edited by G. LI.Tsinghuna University Press, Beijing, pp.490-498.

Chanson H, Cummings PD (1996). Air-Water Interface Area in Supercritical Flows down Small-Slope Chutes. Research Report No. CE151, Dept of Civil Engineering, University of Queensland, Australia, P. 60.

Chanson H, Toombes L (2002). Air-Water Flows down Stepped Chutes: Turbulence and Flown Structure Observations. Int. J. Multiphase Flow. 28(11):1737-1761.

Chanson H, Toombes L (2004). Hydraulics of Stepped Chutes: the transition flow. J. Hydr. Res. 42:43-54.

Chanson H, Carosi G (2007a). Advanced post-processing and correlation analyses in high-velocity air–water flows. Springer, J. Environ. Fluid Mechanics, 7:495–508.

Chinnarasri C, Wongwises S (2006). Flow patterns and energy dissipation over various stepped chutes, J. Irrig. Drain. Eng. 132(1):70–76.

Christodoulou GC (1993). Energy Dissipation on Stepped Spillways, J. Hydr. Eng. A.S.C.E. 19(5):644-650.

El-Kamash MK, Loewen MR, Rajaratnam N (2005). An Experimental Investigation of jet flow on a stepped chute, J. Hydr. Res. 43:31-43.

Gonzalez CA (2005). An Experimental Study of Free-Surface Aeration on Embankment Stepped Chutes, Ph.D. Thesis, Department of Civil Engineering, The University of Queensland, Brisbane, Australia, P.240.

Peterka AJ (1953). The effect of entrained air on cavitation pitting, Joint Meeting Paper, IAHR/ASCE, Minneapolis, Minnesota, Aug.

Peyras L, Royet P, Degoutte G (1991). Ecoulement et Dissipation sur les Déversoirs en Gradins de Gabion (Flow and Energy Dissipation of Energy on Gabion Weirs), La Houille Blanche, 1:37-47.

Rajaratnam N (1990). Skimming Flow in Stepped Spillways. J. Hydr. Eng. 116(4):587-591.

Relvas AT, Pinheiro AN (2011). Stepped chutes lined with wedge-shaped concrete blocks: Hydrodynamic pressures on blocks and stability analysis, Can. J. Civ. Eng. 38(3):338–349.

Sorensen RM (1985). Stepped Spillway Hydraulic Model Investigation, J. Hydr. Eng. ASCE. 11(12):1461-1472.

Toombes L (2002). Experimental Study of Air-Water Flow Properties on Low-gradient Stepped Cascades. Ph.D. thesis, Dept of Civil Engineering, University of Queensland, Brisbane, Australia.

Toombes L, Chanson H (2008). Flow patterns in nappe flow regime down low gradient stepped chutes, J. Hydr. Res. 46(1):4–14.

Wood IR (1991). Air Entrainment in Free-Surface Flows, IAHR Hydraulic Structures Design Manual, No. 4, Hydraulic Design Considerations, Balkema Publ., Rotterdam, The Netherlands, P.149.

Yasuda Y, Chanson H (2003). Micro -and Macro-Scopic study of two-phase flow on a stepped chute, Proc. XXX IAHR Congress, Thessaloniki, Greece, 695-703.

academicJournals

Vol. 8(25), pp. 1371-1373, 9 July, 2013
DOI: 10.5897/IJPS09.187
ISSN 1992-1950 © 2013 Academic Journals
http://www.academicjournals.org/IJPS

International Journal of Physical Sciences

Short Communication

The ability to use light emtting diode (LED) as emergency, instead of gas lamp or tingistin lamp in home lighting

Jassim M. Najim

Department of Physics, KHAWLAN Faculty of Education Arts and Science, Sana'a University, Yemen.

Accepted 1 July, 2013

An electric circuit was made and connected to an alternative current that was passing through lower transformer. This process would produce a current the value of which was 500 mA and a voltage of 6 volt was used to charge battery. When the voltage source (alternative current) was cut, the circuit started lighting. We measured the charge and discharge in addition to time lapses to compare them with the results of the experiment. The results were presented and discussed to compare them with the spent energy in tingistin lamp or gas lamp.

Key words: Electric circuit, light emtting diode (LED) as emergency, instead of gas lamp or tingistin lamp, low energy consumption.

INTRODUCTION

Light emitting diode (LED) lighting has been around since the 1960s, but is just now beginning to appear in the residential market for space lighting. A LED is a special type of semiconductor diode-like a normal diode, it consists of a chip of semicoducting material impregnated, or doped, with impurities to create a structure called a p-n junction. A LED is a semiconductor diode that emits light when an electrical current is applied in the forward direction of the device, as in a simple LED circuit. The effect is a form of electroluminescence where an incoherent and narrow-spectrum light is emitted from the p-n junction. When the voltage across the LED in this case is fixed for the emitted photons, this form releases, when charge-carriers (electron and hole) are created by an electric current passing through the junction, when electron meets a hole it falls into a lower energy level, and releases energy in the form of a photon. When the voltage across the p-n junction is in the correct direction, a significant current flows and the device is said to be forward-biased. But if the voltage is of the wrong polarity, the device is said to be revers biased, very little current flows, and no light is emitted (Jassim, 1999, 2008, 2009; Chih-Hsuan et al., 2008). The wavelength of the light emitted, and, therefore, its color, depends on the bandgap energy of materials forming the p-n junction. A normal diode, typically made of silicon or germanium, emits in a visible faro infrared light, but materials, used for a LED have bandgap energies corresponding to near-infrared, visible or near-ultraviolet light. White light can be produced by mixing differently colored light, the most common method is to use red, green, and blue (RGB). Hence the method is called multi-colored white LED, (sometimes referred to as RGB led) (Hilmi, 2007; Hirosaki et al., 2005). The rising cost of energy also makes the use of LEDs in commercial crop culture imminent. With their energy efficiency, LEDs have opened new perspectives for optimizing the energy conversion and the nutrient supply both on and off Earth.

E-mail : alcedik@yahoo.com.

PACS: 7.50,68.35,85.40,71.30.

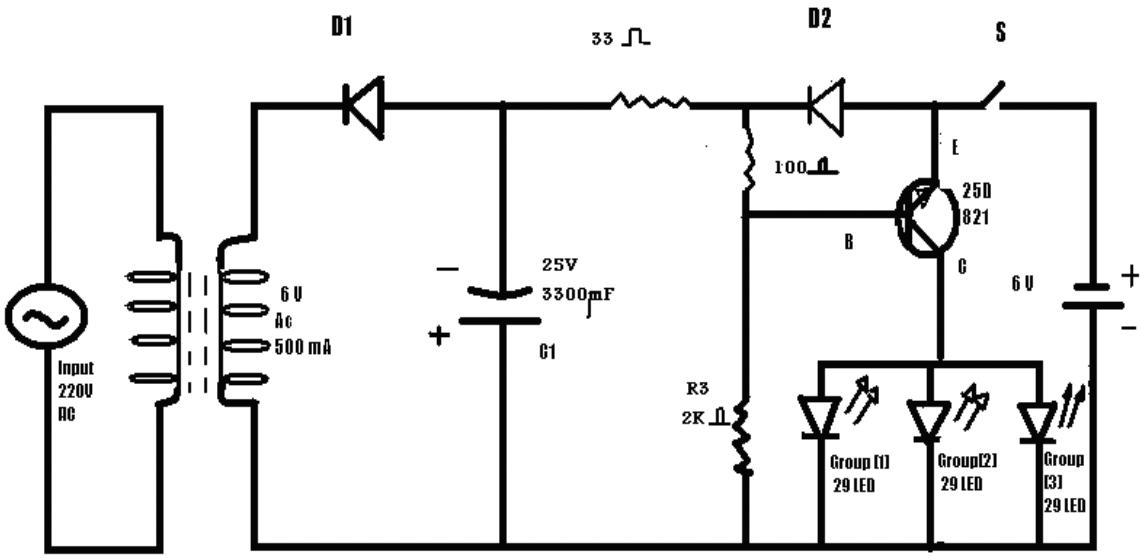

Figure 1. Electric circuit illustrate who we use lighting emitting Diode [LED] as emergency or instead of gas lamp or in home lighting.

EXPERIMENT

Step 1: Making an electric circuit

We made an electric circuit as illustrated in Figure 1. This circuit was connected with an alternative current of 220 voltage that passed through the lower transformer producing a current of 500 mA and 6 volt that passed through diode D1 and at the same time charged the capacity C1 and this capacity regulates the half –wave rectifier to get good direct current (D.C). After that it passed through diode D2. At this time diode D2 is in forward bias to charge the battery through resistance R1. This will result in inducing voltage on diode D2 and would be in the emitte-base of the transistor in off situation. In this case the light emitting diode (LED) would give light, when the source voltage was cut the transistor T1was changed to ON situation after providing the transistor T1 with current base through resistance R3, then the transistor would go to ON situation and light emitting diode (LED) would be in light situation (Figure 1). When the source voltage came again the transistor changed to Off situation and the group of LED changed through R1 and diode D2 and so on. This time we wanted to indicate that if we remove the battery and the electric circuit that was connected direct to alternative current through transformer, the current would be available all the time and emergency situation would be cancelled.

Step 2: Charging battery

As can be seen in Figure 2 the time needed to charge battery was 6 h, after that we see saturation. The time constant of the circuit was equal to the multiplication of C1 by R1, therefore, we must put a suitable value for C1 and R1 in accordance with entering time signal to charge the capacity.

Step3: Discharge statement

In this situation lighting extended to three groups of LED, each group contained 29 leds. Here, by lighting is meant the process of discharge of current coming from the battery charged of 6 volte.

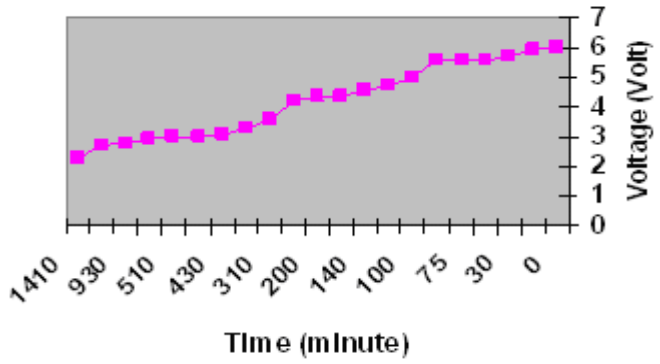

Figure 2. Charge battery.

The results (Figures 3 and 4) showed that we got a twenty three - hour discharge (lighting) which represented the amount of the battery energy spent by the three LED groups.

DISCUSSION

The experiment results, as shown in Figures 1, 2, 3 and 4, explain the possibility of using LED to produce light at home or in the street etc. The energy-saving capacity of LED lights means that they are better for the environment than traditional forms of lighting, and they keep energy bills lower. LEDs last for a long time, typically far longer than fluorescent bulbs. LED lamps have many advantages over traditional lighting methods, these include:

1. Low energy consumption (Figures 3 and 4) the energy

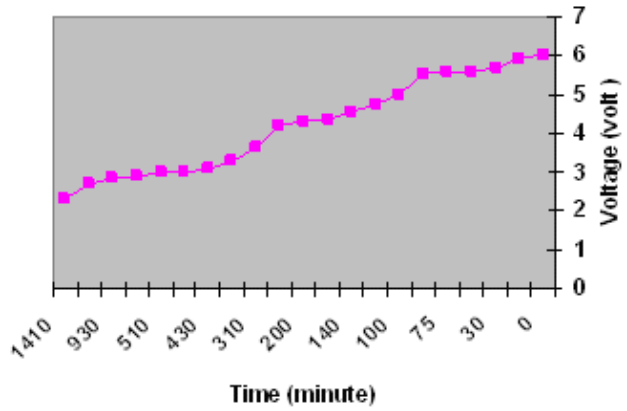

Figure 3. The relationship between the voltage and time (discharge), the decreasing it means LED lighting.

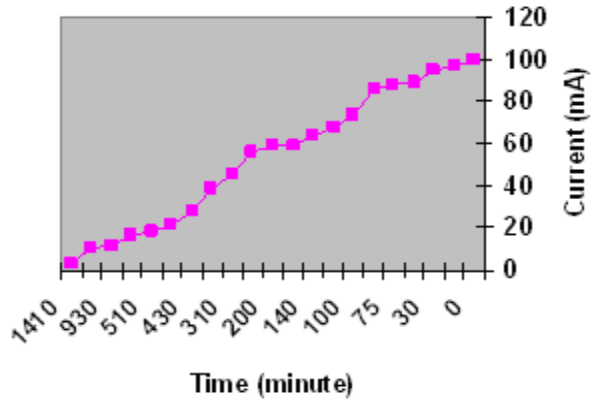

Figure 4. The relationship between the current and the time, the decreasing it means LED lighting.

consumption proximity was 3 watt.

2. LEDs can have a relatively long useful life than incandescent or fluorescent lighting; as we see in Figures 3 and 4 the discharge of battery proximity was 24 h. This electronic circuit is scientifically successful because it needs a long time to unload electric charge.

3. Range of color –LEDs can be manufactured to produce all colors of the spectrum without infared or ultraviolet radiation. The solid package of the LED can be designed to focus its light. Incandescent and fluorescent sources often require an external reflector to collect light and direct it in a usable manner.

4. Durable-LED bulbs are resistant to thermal and vibrational shocks and turn on instantly from -40 to 185°C, making them ideal for applications subject to frequent on-off cycling.

5. No mercury is used in the manufacturing of LEDs.

Conclusion

The results of this study proves that it is possible to use LED for generating light needed in any place. It is also found that in future other resources, other than electricity energy, can be used to produce light by resorting to LED, simply because it consumes very little amount of power to produce light. White LED is well known as a promising device for solid state lighting. It has the advantages of long life, good endurance of heavy impact, no mercury containing and potentially high efficiency. We measured the charge and discharge in addition to time lapses to compare them with the results of the experiment. The results were presented and discussed to compare them with the spent energy in tingistin lamp or gas lamp. However, light output from LED lamp is usually less than 3W, which is very small if compared with traditional light sources and the time of discharge is 23 h. In this article, we will present a new electronic circuit design LED module, with the normal size for lighting purpose. Because of the low power requirement for LEDs, using solar panels becomes more practical and less expensive than running an electric line or using a generator for lighting in remote or off-grid areas. LED light bulbs are also ideal for use with small portable generators which home owners use for backup power in emergencies. More than one – fifth of US electricity is used to power artificial lighting. Light-emitting diodes based on group lll/nitride semiconductors are bringing about a revolution in energy-efficient lighting since the development of incandescent light bulbs in the late 1800s, various methods of producing white light more efficiently have been investigated. Of these, white-light sources based on light-emitting diodes (LEDs) look set to have a considerable impact on issues such as energy consumption, environment and even the health of individuals (Siddha et al., 2009).

REFERENCES

Chih-Hsuan T, Jui-Wen P, Wen-Shing S (2008). Simulating the illuminance and the efficiency of the LED and fluorescent lights used in indoor lighting design. Opt. Express, 16(23):18692-18701.

Hilmi VD (2007). White light generation tuned by dual hybridization of nanocrystals and conjugated polymer, New J. phys. 9:362.

Hirosaki N, Rong J, Kimoto K, Sekiguchi T (2005). Characterization and Properties of green- emitting beta-SiAlon:EU2+ Powder phosphor for white light emitting diode. Appl. phys. lett. (USA)86:211905-1-3.

Jassim MN (1999). Studying the effect Beta and Gamma radiation on the electrical properties of diode ,Zener diode and transistors, Iraqi. J. Sci. 4:40C.

Jassim MN (2008). Studying the effect of X-ray Radiation on the electric properties of diode 1N1405. Int. J. Nanoelectronics Mater. 1:35-39.

Jassim MN (2009). Studying the different effects of Gamma and X-ray Irradiation on Electrical Properties of Silicon diode type 1N1405, Int. J. Nanoelectronics Mater. 2:41-46.

Siddha P, James SS, Steven PDB, Shuji N (2009). Prospects for LED lighting. Nature photonics. 3:180-182.

UPCOMING CONFERENCES

ICNMB 2013 : International Conference on Nuclear Medicine and Biology Switzerland, Zurich, July 30-31, 2013

International Conference on Mathematical Modeling in Physical Sciences Prague, Czech Republic, September 1-5, 2013

Conferences and Advert

July 2013
ICNMB 2013 : International Conference on Nuclear Medicine and Biology
Switzerland, Zurich, July 30-31, 2013

September 2013
International Conference on Mathematical Modeling in Physical Sciences
Prague, Czech Republic, September 1-5, 2013

International Journal of Physical Sciences

academicJournals